https://doi.org/10.5194/egusphere-2026-2222
Preprint. Discussion started: 24 April 2026

Spurious seasonality of Earth observation LAI across three northern evergreen needleleaf forests: Implications for analyses of the carbon cycle

Tim J. Green[1], David T. Milodowski[1], T. Luke Smallman[1,2], Annikki Mäkelä[3], and Mathew Williams[1,2]

[1]School of GeoSciences, University of Edinburgh, Edinburgh, UK
[2]National Centre for Earth Observation, University of Edinburgh, Edinburgh, UK
[3]Department of Forest Sciences, University of Helsinki, Helsinki, Finland

Correspondence: Tim J. Green (tim.green@ed.ac.uk)

Abstract. Leaf area index (LAI) is a key biophysical variable which quantifies the surface area for light capture and photosynthetic activity per unit ground area, giving a first order constraint on potential photosynthesis. LAI is tightly coupled to the carbon, energy, and water cycles of the global terrestrial system. Numerous Earth observation (EO) products provide estimates of LAI over time (LAI_{EO}), delivering valuable information on plant phenology and canopy dynamics. Widely-used LAI_{EO}, however, consistently exhibit unrealistic seasonality in evergreen needleleaf forests at the northern latitudes. Taking a model-data fusion approach, we show that naïvely assimilating biased, whole-year LAI_{EO} (i.e., the business-as-usual (BAU) approach) at three well-studied evergreen needleleaf forests in Fennoscandia implies an ecosystem carbon cycle which is unrealistic and inconsistent with independent lines of evidence. We further demonstrate that the model-data fusion framework, CARDAMOM, is capable of diagnosing realistic seasonal amplitudes of LAI by assimilating localised information on leaf lifespan coupled with summer-only LAI_{EO} (i.e., the alternative (ALT) approach). Important differences arise from the BAU and ALT experiments. The BAU experiment showed highly seasonal canopy dynamics and diagnostic leaf traits erroneously consistent with deciduous species. Conversely, the ALT experiment displayed canopy dynamics and functional characteristics more reflective of evergreen needleleaf species. For BAU, biases in LAI_{EO} propagated throughout the carbon cycle, especially in the southern, more productive sites. This investigation highlights the need for improved LAI_{EO} estimates in northern evergreen forests to enhance understanding of carbon cycle processes in this region of rapid warming and large carbon stores, and provides a mechanism for improvement using independent leaf trait data.

1 Introduction

Leaf area index (LAI) is a key variable describing the amount of photosynthetically active material present in a given environment. Formally defined as one half of the total green leaf area per unit horizontal ground area (Chen and Black, 1992), LAI is an integral component in the study of the terrestrial carbon cycle. LAI is strongly linked to processes such as photosynthesis, respiration, transpiration, and energy exchange (Fang et al., 2019). LAI is a highly dynamic property, varying in both space and time. Consequently, LAI changes provide information on vegetation phenology – the timing of biological events such as

https://doi.org/10.5194/egusphere-2026-2222
Preprint. Discussion started: 24 April 2026

bud burst and leaf senescence (Verger et al., 2016). Due to its high information content, LAI has been deemed an "essential climate variable" by the Global Climate Observing System (WMO et al., 2022), and its use is ubiquitous in the study of land-atmosphere interactions. Terrestrial biosphere models (TBMs) commonly implement LAI in predictions of energy and matter exchanges between the atmosphere and biosphere (Fisher et al., 2014).

The terrestrial carbon cycle is one of the largest sources of uncertainty in future climate projections (Friedlingstein et al., 2014; Piao et al., 2020), underpinning the importance of TBM development and understanding their underlying sources of uncertainty. Model-data fusion (MDF), an inverse calibration technique which varies model parameters based on assimilated observations (Scholze et al., 2017; Wang et al., 2009), has become an increasingly popular tool for evaluating and calibrating TBMs. Bayesian MDF approaches allow for the explicit quantification of uncertainty in model parameters and outputs and are therefore capable of identifying key sources of uncertainty and improving knowledge of ecosystem function and its controls (e.g., Xiao et al., 2014; Keenan et al., 2012; Bloom et al., 2016). While MDF is a valuable tool for carbon cycle analyses, the approach is greatly dependent on observational fidelity. The assimilation of systematically biased observations can propagate errors into outputs, hindering knowledge gain (MacBean et al., 2016). To better predict changes in the terrestrial carbon cycle, MDF frameworks that assimilate LAI require observations which are non-biased and accompanied by robust estimates of uncertainty.

Recent decades have seen the release of numerous Earth observation LAI products (LAI_{EO}) that provide global coverage at moderate resolutions (Fang et al., 2019). LAI_{EO} estimates are typically derived from surface or top-of-atmosphere reflectances measured by passive optical sensors onboard satellites. Observational operators (e.g., machine learning algorithms, inverted radiative transfer models) convert the observed reflectance information into an estimate of LAI (Fuster et al., 2020; Yan et al., 2016). Product updates and new releases typically coincide with new satellite missions or improved algorithms. Widely used LAI_{EO} products include NASA's MCD15A2H (Myneni et al., 2021) derived from the Moderate Resolution Imaging Spectro-radiometer (MODIS) and Copernicus CGLS 300m (Fuster et al., 2020) derived from the Project for On-Board Autonomy – Vegetation (PROBA-V) satellite instrumentation. The short ($\sim$ weekly) revisit times of these satellites allow for LAI estimation at temporal resolutions consistent with rates of phenological change. Currently, LAI_{EO} have been used to assess TBM estimates of carbon cycling globally and across various biomes and land cover types (Jarlan et al., 2008; Li et al., 2019).

Despite their strengths, LAI_{EO} products have been widely evaluated and shown to display significant biases. For example, LAI_{EO} exhibit consistent unrealistic seasonal behaviour in northern evergreen needleleaf forests (ENFs) (Cohen et al., 2006; Heiskanen et al., 2012; Tian et al., 2004). The erroneous seasonality is illustrated by large intra-annual amplitudes, the difference between annual maximum and minimum values. The large amplitudes are linked to implausibly low winter, spring, and autumn LAI values given the dominance of evergreen species. In a recent global analysis of LAI_{EO}, Fang et al. (2021) showed that mean monthly values of MODIS LAI (MCD15A2H) over the ENF biome (2003–2017) was highly seasonal, increasing seven-fold from 0.41 $m^2\,m^{-2}$ in January to 2.95 $m^2\,m^{-2}$ in July and decreasing to 0.28 $m^2\,m^{-2}$ by December. The issue of LAI_{EO} seasonality has long been recognised; however, no significant improvements have been made despite new product releases and updates. For example, at three Fennoscandian sites known to be dominated by evergreen needleleaf species, the

https://doi.org/10.5194/egusphere-2026-2222
Preprint. Discussion started: 24 April 2026

most recent MODIS and Copernicus LAI products show highly seasonal LAI trajectories with amplitudes increasing north to south (Figure 1).

Several explanations for the seasonal behaviour have been offered including: the effect of understory vegetation, cloud and snow contamination, low solar angles, and seasonal variations in chlorophyll content (Chen, 1996; Fang et al., 2019; Weiss et al., 2007; Wang et al., 2017). LAI_{EO} product validation with field-based estimates is typically restricted to a single observation at or near peak growing season (summer), providing information on annual maximum LAI but no constraint on seasonal dynamics (e.g., Garrigues et al., 2008). Regardless of the underlying causes, when used for model calibration, these biases could potentially propagate into MDF carbon cycle analyses in the northern regions. Likewise, when used in evaluation of TBMs, LAI_{EO} biases may drive model development towards ecologically unrealistic outcomes which is especially problematic for this region that is experiencing rapid warming (Post et al., 2019) and holds large amounts of carbon (Bradshaw and Warkentin, 2015; Pan et al., 2024).

Across much of the northern latitude forests where short growing seasons and low soil fertility tend to favour conservative resource investment strategies (Wright et al., 2004), evergreen needleleaf species dominate. Conservative strategies manifest in plant functional traits as high leaf mass per area (LMA), low foliar photosynthetic capacities and nitrogen concentrations, and long leaf lifespans (LLs), all of which are highly correlated and partially form the leaf economics spectrum (Reich et al., 1992; Wright et al., 2004). Of these traits, leaf lifespan has a direct impact on the seasonal variability of LAI (Chen, 1996). Relative to deciduous species which shed their entire canopy each year (LL $<$ 1 year), the long leaf lifespans of northern evergreen needleleaf species equate to low canopy turnover rates, thus low seasonal LAI amplitudes. Leaf lifespan information could therefore be ingested into MDF frameworks to inform modelled canopy turnover and improve representations of LAI seasonal dynamics.

Here, we investigate the implications of incorporating spuriously seasonal LAI_{EO} on carbon cycle analyses by performing two model-data fusion experiments at three northern latitude sites dominated by evergreen needleleaf species. We compare the outputs of a business-as-usual (BAU) experiment that assimilates whole-year LAI_{EO} observations against an alternative (ALT) experiment that assimilates site-specific leaf lifespan information along with summer-only LAI_{EO} to provide constraints on canopy turnover and the annual upper bound of leaf area. We compare diagnostic LAI from BAU and ALT experiments against time series of independent field-based datasets. Two of the test sites contain repeat estimates of LAI spanning the whole growing season, uniquely enabling such an evaluation. Model-data fusion is performed using the CARDAMOM framework (Bloom et al., 2016) that retrieves parameters (i.e., ecosystem functional characteristics, such as LMA, potential photosynthesis rates (PPRs), leaf lifespan) for an intermediate complexity model of the terrestrial ecosystem (DALEC). Using the CARDAMOM-retrieved ecosystem functional characteristics, DALEC is used to diagnose ecosystem carbon stocks and fluxes. This setup allows for insights into LAI_{EO} bias impacts on both trait retrievals and overall carbon cycling. There is potential for LAI biases to influence carbon cycling more broadly than within the canopy alone, for instance adjusting fluxes to and from other plant pools and dead organic matter. Specifically, we will address the following research questions, testing their associated hypotheses:

1. Can the assimilation of local leaf lifespan generate realistic seasonal fluctuations of diagnostic (modelled) LAI? (RQ1)

https://doi.org/10.5194/egusphere-2026-2222
Preprint. Discussion started: 24 April 2026

H1: The assimilation of local leaf lifespan and peak growing season LAI_{EO} will provide significant constraint on canopy turnover resulting in diagnostic LAI consistent with field observations of northern evergreen needleleaf forest LAI.

2. How do biases in whole-year LAI_{EO} affect diagnostics of carbon cycle dynamics and functional characteristics compared to those corrected by leaf lifespan? (RQ2)

H2: The assimilation of whole-year LAI_{EO} will result in canopy dynamics and functional characteristics erroneously indicative of a deciduous system to fit the highly seasonal LAI_{EO} observations. Leaf lifespan corrected analyses will generate canopy characteristics consistent with field observations of evergreen needleleaf species.

H3: Impacts of LAI_{EO} biases will not be limited to canopy carbon dynamics but will propagate throughout the carbon cycle. Differences in whole-system carbon cycling between experiments will be most apparent at southern sites as they exhibit the highest degree of LAI_{EO} seasonal bias, quantified by seasonal amplitude.

2 Methods

2.1 Model and calibration system

We employed a MDF framework, CARDAMOM, to calibrate a process-based model of the terrestrial carbon cycle, DALEC, forced with meteorological data. CARDAMOM assimilates ecological observations to generate data-informed, diagnostic analyses of carbon cycling. DALEC parameters are linked to specific processes, retrieved uniquely for each location and so are ecologically meaningful and reflect biodiversity. Hence parameters are hereafter also referred to as ecosystem functional characteristics. Assimilated ecological observations in this study include: LAI_{EO}, net ecosystem exchange (NEE), wood carbon stock, soil organic matter (SOM) carbon stock, and leaf lifespan. Observations of LMA and foliage litter production were left out of the assimilation to be used for independent model evaluation. CARDAMOM calibrated DALEC based on a weekly time step across four years (2016 – 2019) independently at each of the three sites in this study.

2.1.1 DALEC

The DALEC suite of intermediate complexity terrestrial ecosystem models are capable of simulating both carbon and water cycles (Bloom and Williams, 2015; Smallman and Williams, 2019; Williams et al., 2005). Currently the suite is comprised of more than 15 published versions of DALEC (Famiglietti et al., 2021; Smallman et al., 2021). In this analysis we specifically use DALEC4. DALEC4 has previously been described as M3 in Smallman et al. (2021) and C7 in Famiglietti et al. (2021). DALEC4 (hereafter referred to simply as DALEC) simulates the flow of carbon through four live biomass pools (foliage, labile, fine roots, wood) and two dead organic matter pools (DOM): litter and SOM. All fluxes are donor-controlled by calibrated parameters.

https://doi.org/10.5194/egusphere-2026-2222
Preprint. Discussion started: 24 April 2026

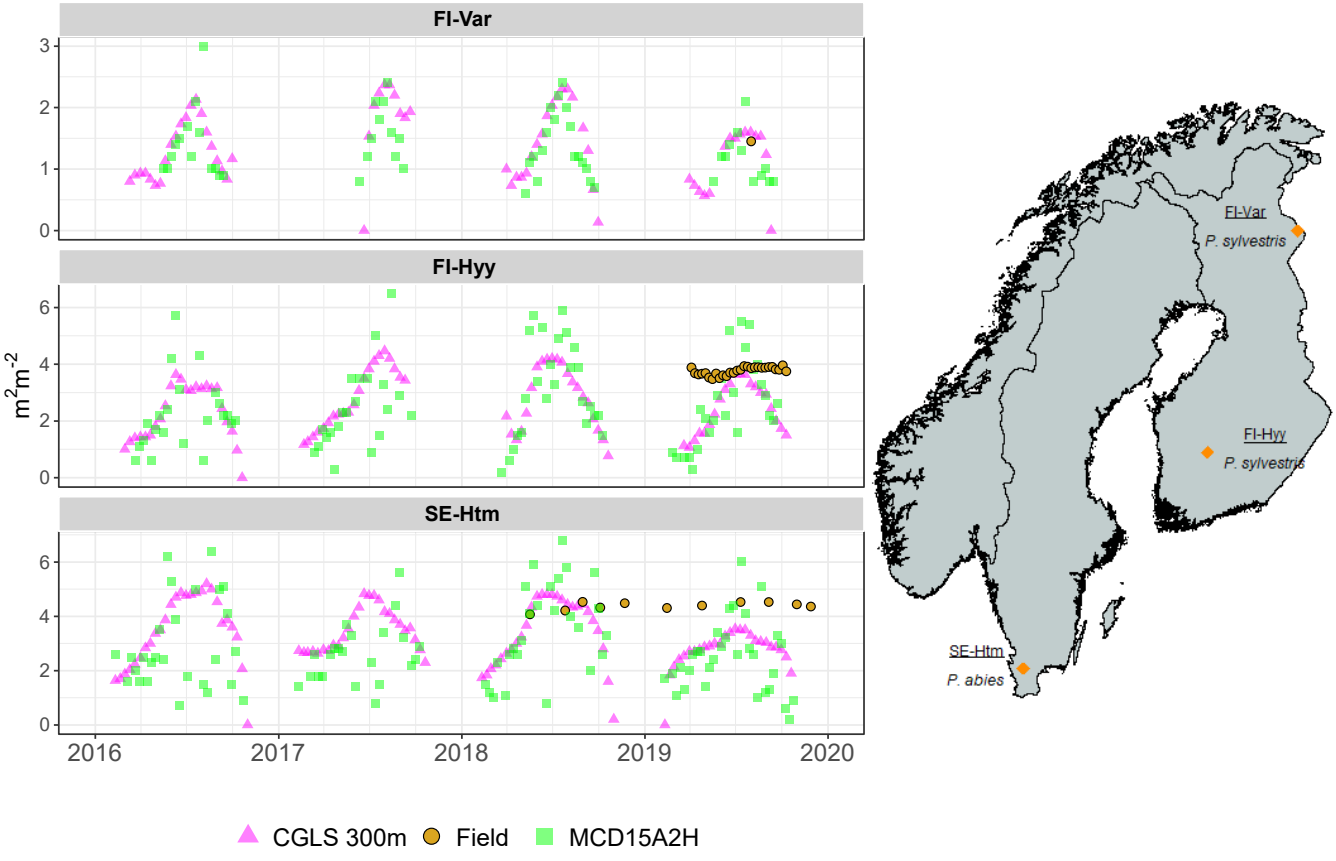

Figure 1. Seasonal trajectories of Earth observation LAI (CGLS 300m [purple triangles]; MCD15A2H [green squares]) and field LAI [gold circles] at three Fennoscandian sites dominated by evergreen needleleaf species (2016-2019). Field values at FI-Var (n=1) and SE-Htm (n=11) are derived from digital hemispheric photography. At FI-Hyy (n=28), field values are based on below- and above-canopy PAR sensors and the inverted Beer-Lambert equation with a local extinction coefficient. Dominant species at each site are noted on the map.

Carbon enters the system via gross primary productivity (GPP), which is a function of LAI, plant functional characteristics (e.g., potential photosynthetic rate (PPR), rooting depth), soil moisture, and meteorology. The PPR parameter sets the upper limit of GPP which is then downregulated by the co-limitation of temperature, light, and atmospheric CO_2 availability. A fraction of GPP is lost to the atmosphere as autotrophic respiration (R_a). The remainder supports net primary productivity (NPP). Carbon use efficiency (CUE, 0–1) determines the fractional partitioning of GPP to R_a and NPP (NPP = GPP · CUE). NPP is allocated to the live biomass pools by calibrated fixed fractions. Foliage can receive carbon directly from NPP or via the labile pool. Allocation via the labile pool occurs during a flushing period, the peak timing and total duration of which are controlled by calibrated parameters. Foliage senescence is also calibrated, determined by parameters that define the peak

https://doi.org/10.5194/egusphere-2026-2222
Preprint. Discussion started: 24 April 2026

timing and duration of a leaf fall period. Modelled LAI is determined by the size of the foliage pool and LMA. LMA is a calibrated parameter.

Turnover of the fine root and woody pools are continuous processes controlled by calibrated fixed fractions. Turnover from foliage and fine root feed into the litter pool, while wood turnover supports the SOM pool. Litter decomposition to SOM and mineralisation of litter and SOM to heterotrophic respiration ($R_{h\text{-litter}}$ and $R_{h\text{-SOM}}$, respectively) each follow parameterised first order kinetics modified by an exponential temperature coefficient. Collectively, $R_{h\text{-litter}}$ and $R_{h\text{-SOM}}$ comprise total heterotrophic respiration (R_h). The sum of R_a and R_h is total ecosystem respiration (R_{eco}).

2.1.2 CARDAMOM calibration system

CARDAMOM (Bloom et al., 2016; Worden et al., 2025) is the MDF framework that calibrates DALEC. Taking a Bayesian approach via an adaptive proposal Markov chain Monte Carlo (AP-MCMC) algorithm (Haario et al., 2001), CARDAMOM varies model parameters to minimize the mismatch between simulated model states (and/or fluxes) and their concomitant observations, weighted by associated observational uncertainty. Following Bayes' theorem, given a parameter vector, X, and a set of observations, O, with uncertainty, σ, the probability of the parameter vector given the observations, P(X|O), is calculated as a function of the likelihood of the observations given the parameter set, P(O|X), and any prior knowledge on the parameter distributions, P(X):

$$P(X \mid O) \propto P(O \mid X) \cdot P(X) \tag{1}$$

The likelihood, P(O|X), is calculated based on the mismatch between N available observations and their equivalent modelled state or flux values, M, produced by the current parameter vector, X:

$$P(O \mid X) = \exp\left(-0.5 \cdot \sum_{n=1}^{N} \left(\frac{O_n - M_n}{\sigma_n}\right)^2\right) \tag{2}$$

Prior knowledge, P(X), on parameter ranges are intended to span plausible (observable) ranges (e.g., non-negative turnover rates). Specific prior distributions can also be placed on parameters, for instance Gaussian priors provided for CUE (0.46 ± 0.12) (Collalti and Prentice, 2019) and PPR (21.15 ± 8.53 g C m^{-2} leaf day^{-1}) (Kattge et al., 2020). Ecological theory which cannot be readily described as a numerical prior is incorporated with ecological and dynamical constraints (EDCs) (Bloom and Williams, 2015). EDCs are a set of rules that ensure ecological realism in the absence of observational constraint by rejecting parameter sets that result in ecologically unrealistic outputs. EDCs provide constraint on carbon pool turnover times and the relationship between emergent dynamics of live biomass pools. EDCs also prevent unrealistic fluctuations in wood, litter, and SOM pools in the absence of disturbance.

A subset of calibrated parameters include the initial states of all carbon pools and an initial soil water parameter. These parameters align with the state value at time step = 1 of an analysis. By calibrating initial states, CARDAMOM is able to forego model spin-up, the standard practice of running models over long time scales to bring pools into equilibrium with

https://doi.org/10.5194/egusphere-2026-2222
Preprint. Discussion started: 24 April 2026

environmental forcing. See Table A1 for further details on all calibratable parameters. In this study, 100 accepted parameter vectors were sampled from the latter half of three independent AP-MCMC chains. CARDAMOM then produced an ensemble of modelled fluxes and states at every time step, explicitly capturing uncertainty in outputs.

2.2 Experimental setup

We ran two independent CARDAMOM assimilation experiments (Table 1), generating two diagnostic carbon cycle analyses at each of the three sites included in this study. The first experiment, BAU (business-as-usual), assimilated all available LAI_{EO} observations from the CGLS 300m product (Fuster et al., 2020), which exhibit seasonal bias (Figure 1). The second experiment, ALT (alternative), assimilated local information on leaf lifespan and CGLS 300m LAI from the summer period only (DOY 168–231, inclusive), removing the majority of seasonally biased observations. We assume LAI_{EO} during summer is unbiased and provides adequate constraint on maximum annual LAI. All other assimilated data and meteorological forcing were consistent across the two experiments. Differences in carbon cycle analyses between BAU and ALT can therefore be attributed to the impacts of assimilated LAI and leaf lifespan information.

To assess the constraint on the seasonality of diagnostic LAI resulting from the assimilation of leaf lifespan information (RQ1), we compared diagnostic LAI derived from the two assimilation experiments (BAU and ALT) against independent field-based estimates at the two sites where multiple data were available. To investigate how biases in whole-year LAI_{EO} affect carbon cycle analyses of the entire system (RQ2), we explored differences in diagnostic canopy dynamics, functional characteristics, and carbon fluxes and pools between BAU and ALT at all three sites. Diagnostic outputs from the assimilation experiments are denoted with a subscript of the experiment name. For example, LAI_{BAU} equates to diagnostic LAI derived from the BAU experiment.

Experiment	Assimilated LAI_{EO}	LAI_{EO} temporal filtering	Leaf lifespan assimilated?
BAU	CGLS 300m	none	N
ALT	CGLS 300m	summer-only	Y

Table 1. Assimilation experiments and associated details. BAU = Business-as-usual experiment; ALT = Alternative experiment with summer-only assimilation.

2.3 Site descriptions

Three evergreen needleleaf sites were chosen for this analysis due to their abundant data availability. All sites maintain an eddy-flux tower and are members of the Integrated Carbon Observation System (ICOS) network, thus possessing relevant information suitable for calibrating, driving, and validating DALEC at a weekly time step. The three sites are situated along a latitudinal gradient (56° 6' N – 67° 45' N) (Figure 1, right panel) and experience a wide range of temperature regimes (Table 2). Finnish sites Varrio (FI-Var) and Hyytiälä (FI-Hyy) are dominated by *Pinus sylvestris* L. (hereafter referred to as pine) and

https://doi.org/10.5194/egusphere-2026-2222
Preprint. Discussion started: 24 April 2026

lie within the boreal climate region. In the spring of 2019 at FI-Hyy, the majority of understory trees with a diameter at breast height (DBH) < 7 cm were removed. The thinning had a minor impact on site-level leaf area, reducing field-measured LAI by $0.3\,m^2\,m^{-2}$ (Aslan et al., 2024). The Swedish site, Hyltemossa (SE-Htm), is dominated by *Picea abies* (L.) Karst (hereafter referred to as spruce) and is located within a northern temperate, maritime climate. All sites contain only small proportions of deciduous species ($< 10\%$ of total basal area).

Site	Lat	MAT	MAP	Basal area	Species-specific LL	Effective LL
	°N	°C	mm	$m^2\ ha^{-1}$ (%P, %S, %D)	yrs. (P, S, D)	yrs.
Fl-Var	67.8	0.0	539	15.0 (95, 0, 5)	5.2, NA, 0.4	4.9
Fl-Hyy	61.8	4.7	705	28.6 (82, 9, 8)	3.6, 6.8, 0.5	3.6
SE-Htm	56.1	8.5	745	27.4 (0, 97, 2)	NA, 3.1, 0.6	3.0

Table 2. Summary information for three sites in the analysis. Mean annual temperature (MAT) and mean annual precipitation (MAP) are representative of the four years in this analysis (2016—2019). The species-specific basal area percent is used as the weighting mechanism in the calculation of the effective leaf lifespan observation, see Eq. (4). P = Pine, S = Spruce, D = Deciduous.

2.4 Drivers and observations

All model drivers (meteorology and atmospheric CO_2) and observations of GPP, R_{eco}, NEE, and LMA were taken from the ICOS Warm Winter dataset, downloaded from the ICOS Carbon Portal (Warm Winter Team and ICOS Ecosystem Thematic Center, 2020).

2.4.1 Meteorological drivers

Meteorological forcings required by DALEC include air temperature, atmospheric CO_2 concentration, shortwave radiation, wind speed, precipitation, and vapour pressure deficit at each weekly time step. These drivers are locally derived, based on site-specific measurements at the flux towers.

2.4.2 LAI

Assimilated observations of LAI_{EO} were extracted from the 300 m resolution Copernicus Global Land Service (CGLS 300m) LAI product version 1.0 (Fuster et al., 2020). Top-of-atmosphere reflectances from PROBA-V are converted to LAI with the GEOV3 artificial neural network algorithm (Baret et al., 2016), which is in part trained by the MODIS collection 5 (Yang et al., 2006) and CYCLOPES (Baret et al., 2007) LAI products. Values originating from pixels contaminated with cloud or snow are rejected during product processing. Product processing also includes a temporal smoothing procedure, providing estimates that are more conducive for site-level analyses, contrary to the noisy time series of the MODIS LAI product at pixel scale (Brown et al., 2020). CGLS 300m provides LAI estimates at 10-day intervals. If two LAI_{EO} observations fell within the same weekly time step of the model run, the mean between the two values was taken.

https://doi.org/10.5194/egusphere-2026-2222
Preprint. Discussion started: 24 April 2026

The CGLS 300m product provides uncertainty estimates associated with observations. However, there are times and places for which an LAI estimate is provided but the uncertainty estimate is missing. For missing uncertainty values, we assigned a cautious relative uncertainty of 20% during the summer period (DOY 168–231) and 50% outside summer, with a minimum threshold of 0.2 $\mathrm{m^2 m^{-2}}$. The choice in uncertainty partly reflects the threshold values specified by the Global Climate Observing System (GCOS) Essential Climate Variable (ECV) requirements (WMO et al., 2022). Pixel extraction was based on the coordinates of the flux towers. We restricted the time period of the analysis to 2014—2019 to avoid the sensor transition from PROBA-V to OLCI onboard Sentinel-3 that occurred in 2020.

Independent field-based data sets of LAI ($\mathrm{LAI_{FIELD}}$) at FI-Hyy and SE-Htm were used for evaluation. The field-based dataset at FI-Hyy was derived from above (n = 1) and below-canopy photosynthetically active radiation (PAR) sensors (n = 16) situated near the flux tower. A processed data set was provided by the site data manager (Pasi Kolari) via personal correspondence. Estimates were available every three days (n = 64) from early-April to mid-October, 2019. Processed LAI was calculated based on an inverted Beer-Lambert equation, with an extinction coefficient (0.18) determined at the site in 1998 (Mäkelä et al., 2006). Clumping is implicitly accounted for in the extinction coefficient formulation; however, extinction coefficients are known to vary with stem density across stands of the same species (Smith, 1993). As forest structure has likely changed at FI-Hyy since 1998, the extinction coefficient may no longer be appropriate. However, since the dominant species has not changed during that time period, leaf optical properties have likely remained stable. Absolute values of estimated field LAI may be affected by the extinction coefficient used here, but the seasonal shape should be minimally affected. The three-day estimates were aggregated to the weekly CARDAMOM time step (n = 28; 10 in the summer period, 18 outside the summer period) by taking the mean across the 16 sensor-specific LAI values falling within each week.

To quantify observational uncertainty of $\mathrm{LAI_{FIELD}}$ at FI-Hyy, we calculated the standard deviation of the sample and the standard error of the mean across all estimates falling within each weekly time step. We then added these two sources of uncertainty in quadrature. The mean relative uncertainty across all time steps was 16%. We inflated this value to 21% to account for poorly constrained sources of uncertainty (e.g., instrument error and extinction coefficient uncertainty). The 21% uncertainty was assumed for all weekly aggregated field LAI values at FI-Hyy.

Field-based LAI estimates at SE-Htm were based on digital hemispheric photography (Chianucci, 2020) following ICOS sampling protocols (Gielen et al., 2017). Processing of photographs and quantification of LAI was performed by ICOS. Site-level aggregated data is available from the ICOS data portal (Heliasz et al., 2026). Individual, photograph-specific LAI values were provided by the site manager (Tobias Biermann) via personal correspondence. Photographic campaigns typically provided approximately 35 processed values that were averaged to produce a site-level LAI estimate aligning with a single CARDAMOM weekly time step. We estimated uncertainties by adding the standard deviation of the sample and standard error of the mean in quadrature. Mean relative uncertainty across all time steps was 19% which we inflated to 24% and applied to all observations to account for unconstrained errors.

The field-based LAI data used here are more accurately described as plant area index (PAI) due to the influence of woody components in estimation. Site-specific values of woody area index (WAI) are needed to convert PAI to LAI, which were unavailable at the sites in this analysis. WAI varies considerably both across and within biomes (Fang et al., 2019). Lacking

https://doi.org/10.5194/egusphere-2026-2222
Preprint. Discussion started: 24 April 2026

this information, we neglected a PAI adjustment. However, the impact on seasonal trajectories is most likely minimal given the assumption that the surface area of woody components does not change considerably within a given year (Chen, 1996).

2.4.3 Flux measurements

Half-hourly aggregated estimates of weekly NEE based on the eddy covariance method (Baldocchi, 2003) were obtained from the ICOS data portal. NEE equates to the difference between GPP and R_{eco}, where negative values correspond to net carbon uptake and positive values to net carbon release from land to the atmosphere. R_{eco} is comprised of both autotrophic respiration (R_a) and heterotrophic respiration (R_h).

$$NEE = R_{eco} - GPP \tag{3}$$

Estimates of the component fluxes GPP and R_{eco} are derived from NEE based on the night-time (Reichstein et al., 2005) or daytime (Lasslop et al., 2010) partitioning methods, both made available in the ICOS data. We extracted night-time partitioned fluxes at FI-Hyy and SE-Htm and day-time partioned fluxes at FI-Var as it sits above the Arctic circle and does not experience complete darkness during the peak summer period.

We screened NEE observations based on their associated quality control (QC) values provided by ICOS. The QC value (fraction, 0-1) indicates the amount of measured or good quality, gap-filled half-hourly values within each weekly time period. As GPP and R_{eco} estimates are derived from NEE, all fluxes associated with a NEE QC value < 0.85 were removed from the analysis. A constant observational uncertainty of $0.58\,\mathrm{g\,C\,m^{-2}\,day^{-1}}$ was assumed for each observation of NEE based on the findings of Hill et al. (2012). All screened NEE observations were assimilated and component fluxes GPP and R_{eco} were left out for model evaluation. The percentage of weeks containing NEE observations suitable for assimilation at each site was 96% at FI-Var, 87% at FI-Hyy, and 95% at SE-Htm.

In addition to flux tower observations, we obtained foliage litter trap data at FI-Hyy (2007–2017) and SE-Htm (2019–2022) via personal correspondence with site managers. Measurements from 20 litter traps at each site were averaged across each recording period and then aggregated to one mean annual value of foliage litter production at each site. These estimates were used for independent model evaluation.

2.4.4 Forest inventory

Tree-level inventory data were provided by site managers and used to estimate basal area and wood carbon stock. Tree height, DBH, and species were recorded for every individual > 5 cm DBH within survey plots surrounding the flux tower at each site following ICOS protocols (Gielen et al., 2017). We used species-specific allometric equations (Marklund, 1988; Petersson and Ståhl, 2006) to derive an estimate of total wood stock at each site by summing component biomass estimates of stem and bark, live branches, stump, and coarse roots down to 2 mm diameter. To convert from biomass to units carbon, we assumed a conversion factor of 0.5. One estimate of wood stock was assimilated for each site (FI-Var 2019, FI-Hyy 2018, SE-Htm 2016).

https://doi.org/10.5194/egusphere-2026-2222
Preprint. Discussion started: 24 April 2026

A conservative relative uncertainty of 20% was assumed for each observation of wood carbon stock based on expert advice from site managers.

2.4.5 Soil properties

An estimate of SOM carbon in the surface soil layer (0–30 cm) for each site and its associated uncertainty were extracted from the SoilGrids version 2 product (Poggio et al., 2021), which provides various soil property maps at a 250 m resolution. SoilGrids SOM carbon stock maps are obtained by modelling carbon density at various depths between 0 and 30 cm based on measurements of soil organic carbon concentration, bulk density, and coarse fragment percentage at various sampling locations. SOM carbon stock equates to the weighted sum of the carbon densities for each soil layer. SOM carbon stock estimates from sample locations are then used to create a global map using quantile random forest modelling. We extracted SOM estimates from the SoilGrids global map for each site location based on the flux tower coordinates. Soil texture information required by DALEC was also extracted from the SoilGrids product.

2.4.6 Leaf lifespan

For the ALT experiments, we constructed an observation of the effective leaf lifespan ($LL_{effective}$) for the forest canopy at each site independently. DALEC simulates the entire canopy as one layer. Effective canopy leaf lifespan was calculated as the weighted mean of species-specific leaf lifespans, with weights equal to the proportion of each species' basal area relative to the total basal area at the site when tree inventories were conducted.

$$LL_{effective} = LL_{pine} \cdot W_{pine} + LL_{spruce} \cdot W_{spruce} + LL_{decid} \cdot W_{decid} \quad (4)$$

where W signifies the weighting value for each species classification. Weight values at each site were determined based on the stem inventory (Table 2).

Leaf lifespans are specific to each site location. For pine and spruce, we used the number of needle cohorts as a proxy for leaf lifespan, a common practice in leaf lifespan calculation (e.g., Reich et al., 2014; Jankowski et al., 2017). As one needle cohort is produced each year, the total number of cohorts retained on a branch directly reflects how many years the needles persist before being shed, making it a reliable proxy for leaf lifespan (Muukkonen, 2005). At FI-Hyy and FI-Var, we extracted needle cohort information from Finnish maps generated by Tupek et al. (2015). At SE-Htm, spruce leaf lifespan is based on a needle cohort survey conducted at the site in 2023 (data provided by site manager via personal correspondence). To estimate deciduous leaf lifespan (LL_{decid}), we used growing season length (GSL) as a proxy:

$$GSL = GSE - GSS \quad (5)$$

where GSE is growing season end (DOY), and GSS is growing season start (DOY). We implemented the widely used definitions of GSE and GSS in the Nordic countries described in Venäläinen and Nordlund (1988), where GSS coincides with the point

https://doi.org/10.5194/egusphere-2026-2222
Preprint. Discussion started: 24 April 2026

at which daily mean temperature exceeds 5° C for five consecutive days. GSE is determined when the 10-day rolling average of daily mean temperature drops below 5° C. Site-specific LL_{decid} was calculated using daily mean temperature data from the four years included in this analysis (2016—2019).

$$LL_{decid} = \frac{GSL}{365.25} \tag{6}$$

Effective leaf lifespan information was incorporated in the CARDAMOM calibration by its inclusion in the likelihood function (Eq. 2). $LL_{effective}$ was treated as an observation and compared against its model equivalent (LL_{mod}). LL_{mod} is calculated as the mean foliar pool size across the analysis period divided by mean foliar litter production.

As no raw data were publicly available for the Finnish needle cohort survey presented in Tupek et al. (2015), we assumed uncertainty of $LL_{effective}$ based on survey data presented in Oleksyn et al. (2020). Data included the number of needle cohorts counted from several branches of over 1,300 trees across 74 pine sites in Sweden. Data from Sweden was assumed to be applicable for Finland given similar climates between countries. We calculated uncertainty at each of the 74 sites presented in Oleksyn et al. (2020) by adding in quadrature the standard deviation of values at each site with the standard error of the mean. The mean relative uncertainty across all sites was 10.3%. We inflated this uncertainty to 15%, which was the assumed relative uncertainty for all $LL_{effective}$ values in this study.

2.4.7 LMA

We calculated effective LMA values at each site following the weighted average scheme for effective leaf lifespan. Species-specific estimates of LMA for pine and spruce were taken from ICOS ancillary data at FI-Hyy and SE-Htm (Warm Winter Team and ICOS Ecosystem Thematic Center, 2020). At FI-Var, LMA was provided by the site PI (Pasi Kolari) via personal correspondence. For birch LMA, the main deciduous species at all sites, observations of *Betula pendula* and *Betula pubescens* located in Fennoscandia were extracted from the TRY database (Kattge et al., 2020). The mean of extracted observations (excluding measurements from manipulation experiments, e.g., elevated CO_2) was used as the deciduous LMA value at all sites ($38.3\,\mathrm{g\,C\,m^{-2}\,leaf}$). Species-specific basal areas were used as weights in the effective LMA calculation. Effective LMA was used for independent evaluation of the calibration process.

2.5 Metrics

2.5.1 Model-data fusion assessment

To gauge how well CARDAMOM outputs of diagnostic fluxes and states fit their corresponding observations, we calculated the percentage of output ensemble members generated by CARDAMOM that fall within observational uncertainty bounds at each time step an observation is available. We then took the mean percentage across all time steps for a particular data stream to produce a diagnostic-observation overlap (DOO) percentage. DOO can be calculated with assimilated or independent, non-assimilated observations. DOO accounts for uncertainty in both the outputs and observations they are compared against. In the

https://doi.org/10.5194/egusphere-2026-2222
Preprint. Discussion started: 24 April 2026

following text, DOO is often referred to simply as "overlap". We also calculated the root mean squared error (RMSE) between median values of diagnostic fluxes and corresponding observations of GPP, R_{eco}, and NEE.

2.5.2 Hellinger distance

As CARDAMOM produces an ensemble for every output, outputs can be expressed as probability distributions to explicitly express uncertainty. To quantify differences between diagnostic outputs from the two assimilation experiments (BAU vs. ALT), we employed the use of the Hellinger distance (Hellinger, 1909; Boone et al., 2014), which measures the (dis)similarity between two probability distributions. Properties of the Hellinger distance allow for easy interpretation as it is a bounded metric ranging from 0 to 1, where 0 indicates two identical distributions and 1 indicates completely dissimilar distributions, i.e., the two distributions do not overlap in any region of probability space. Specifically, the Hellinger distance, HD, between two continuous probability distributions, p and q, is defined as

$$\mathrm{HD}(p,q) = \sqrt{\frac{1}{2}\int \left(\sqrt{p(x)} - \sqrt{q(x)}\right)^2 dx} \tag{7}$$

To compute HD between the diagnostic outputs of the experiments, we first approximated probability density functions (PDFs) from the diagnostic ensemble outputs via kernel density estimation (KDE) for bounded densities using the reflection method (Jones, 1993). The reflection method corrects for the allocation of non-zero probability to regions outside plausible bounds (e.g., positive probability attributed to negative values of non-negative data) by mirroring overspilled density back to the bounded range. Here, the reflection method corrects for downward biased PDFs introduced by standard KDE. We used a Gaussian smoothing kernel and bandwidths determined by the Sheather and Jones method (Sheather and Jones, 1991). We used a Hellinger distance value of 0.5 to mark the threshold that designates similarity/dissimilarity between two distributions (similar: $\mathrm{HD} < 0.5$; dissimilar: $\mathrm{HD} > 0.5$).

2.5.3 LAI seasonality

To quantify the degree of seasonality in diagnostic LAI, we computed the absolute seasonal amplitude (ASA) and relative seasonal amplitude (RSA) of LAI for each year in the analysis separately.

$$\mathrm{ASA} = \mathrm{LAI}_{max} - \mathrm{LAI}_{min} \tag{8}$$

$$\mathrm{RSA} = \frac{\mathrm{ASA}}{\mathrm{LAI}_{max}} \tag{9}$$

where LAI_{max} and LAI_{min} are the highest and lowest LAI values in each respective year. RSA, a normalised value, ranges from 0 to 1 where 0 indicates a complete lack of seasonality and 1 indicates high seasonality. We then took the mean ASA and RSA across all years in the analysis at each site and experiment. ASA and RSA are based on the median diagnostic LAI values.

https://doi.org/10.5194/egusphere-2026-2222
Preprint. Discussion started: 24 April 2026

3 Results

3.1 LAI seasonality

Overlap values (DOO) between diagnostic LAI and assimilated LAI_{EO} showed that CARDAMOM adequately fit ingested observations for both the ALT experiment (DOO_{ALT}: FI-Var = 83%; FI-Hyy = 87%; SE-Htm = 84%) and the BAU experiment (DOO_{BAU}: FI Var = 88%; FI-Hyy = 88%; SE-Htm = 84%). High overlap with assimilated observations establishes that the following results are not the consequence of poor model-data fusion performance. LAI_{BAU} satisfactorily reflected whole-year LAI_{EO}, and LAI_{ALT} matched well to the peak summer values of LAI_{EO}.

The assimilation of local leaf lifespan resulted in close agreement between LAI_{ALT} and independent LAI_{FIELD} at FI-Hyy and SE Htm (Figure 2). LAI_{ALT} overlap with field data (DOO_{ALT}: FI-Hyy = 98%; SE-Htm = 96%;) was 38-60% greater than LAI_{BAU} overlap (DOO_{BAU} FI-Hyy = 60%; SE-Htm = 36%). Low DOO_{BAU} with field data was caused by erroneous seasonality indicated by LAI_{EO}.

Differences in the seasonality of LAI_{ALT} and LAI_{BAU} are further quantified by absolute seasonal amplitude (ASA) and relative seasonal amplitude (RSA) (Table 3). Mean RSA_{BAU} across all site years was 0.84, signifying strong seasonal fluctuations in LAI_{BAU}. In contrast, mean RSA_{ALT} was 0.18, indicating a lack of seasonality consistent with expectations for evergreen systems.

Site	ASA_{BAU}	RSA_{BAU}	ASA_{ALT}	RSA_{ALT}
FI-Var	1.67	0.84	0.49	0.25
FI-Hyy	2.80	0.77	0.61	0.17
SE-Htm	4.08	0.90	0.54	0.12

Table 3. Mean annual (2016–2019) absolute seasonal amplitude (ASA) and relative seasonal amplitude (RSA) of diagnostic LAI from both assimilation experiments.

3.2 Canopy carbon dynamics

Seasonal biases in LAI_{EO} propagated into diagnostics of canopy carbon dynamics. Seasonal fluctuations in diagnostic LAI interact with the net balance of carbon inflows (direct NPP allocation, indirect flows from the labile pool) and carbon outflows (foliage litter production). Consequently, the two experiments exhibited differences in carbon inflows and outflows to foliage (Figure 3). $Foliage_{BAU}$ growth in spring was driven by large inputs from the labile pool. At FI-Var, labile inputs accounted for 23% of total annual inflow to $Foliage_{BAU}$ compared with 11% to $Foliage_{ALT}$. Larger differences were observed at FI-Hyy (49% vs. 6%), and SE-Htm (32% vs. 5%). Total canopy outflows in the form of foliage litter production were higher for $Foliage_{BAU}$ across all sites. Relative to ALT, total annual foliar litter production from BAU was 159% (FI-Var), 138% (FI-Hyy), and 69% (SE-Htm) higher when comparing median estimates.

https://doi.org/10.5194/egusphere-2026-2222
Preprint. Discussion started: 24 April 2026

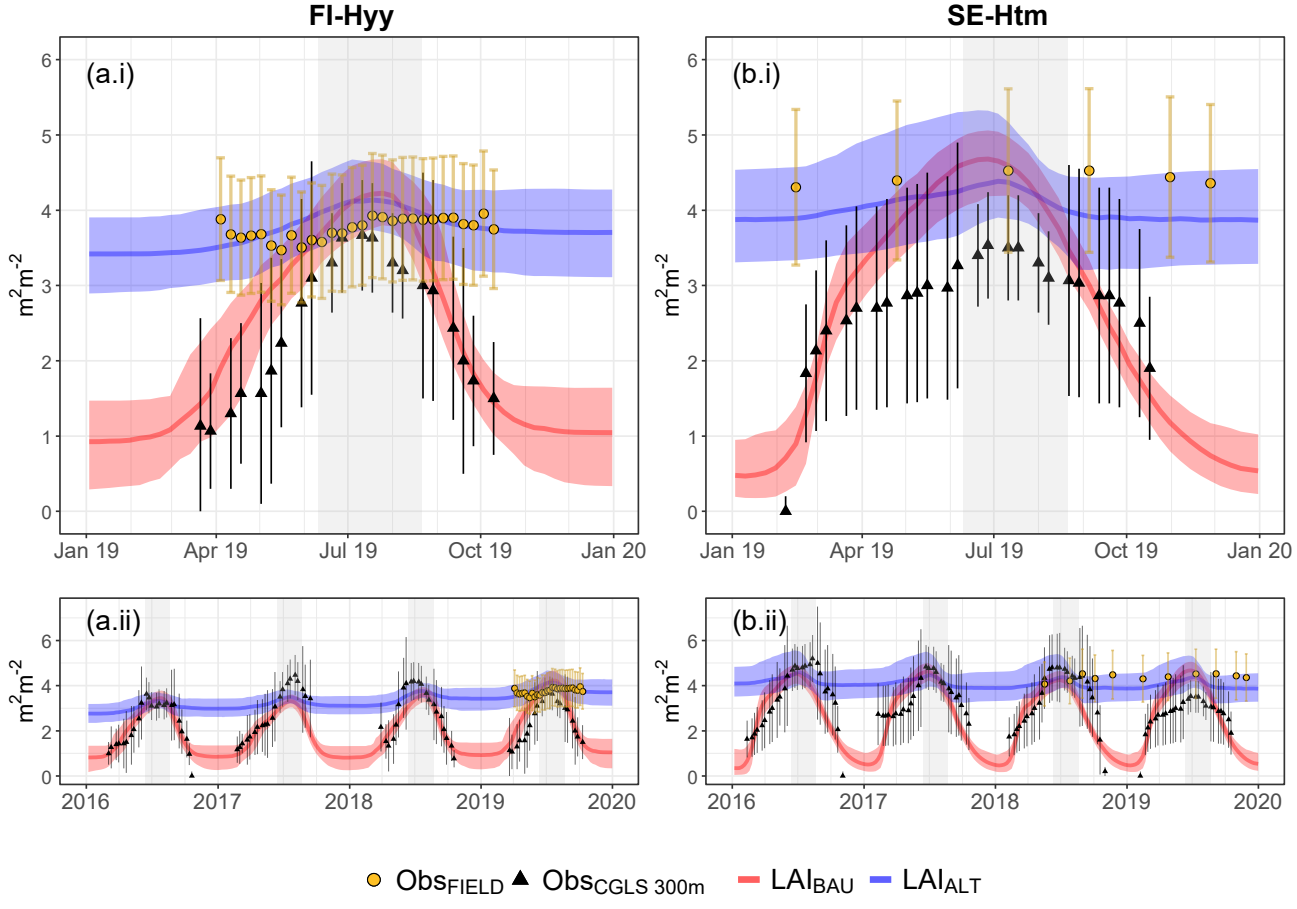

Figure 2. Diagnostic LAI (LAI_{BAU}, LAI_{ALT}), assimilated LAI_{EO} observations ($Obs_{CGLS\ 300m}$), and independent field LAI observations (Obs_{FIELD}) at FI-Hyy (panels a.i and a.ii) and SE-Htm (panels b.i and b.ii). Top panels show results from the year with the most independent field observations (2019). Bottom panels show the entire four year time series of the analysis. Grey shading denotes the summer LAI_{EO} assimilation window for ALT experiments. Coloured lines represent the median LAI estimate from each experiment. Coloured shading represents a 95% confidence interval. Errors bars represent observational uncertainty.

https://doi.org/10.5194/egusphere-2026-2222
Preprint. Discussion started: 24 April 2026

Foliage litter trap data provided independent evaluation of the diagnosed canopy outflows from the two experiments. At FI-Hyy, comparisons show the assimilation of leaf lifespan information improved diagnostic estimates of foliage litterfall. The field-based estimate of mean annual foliage litter production (2007 – 2017) was 88.1 $\mathrm{g\,C\,m^{-2}\,yr^{-1}}$. This value falls outside the 95% confidence interval (95CI) for BAU [118.5 – 391.1 $\mathrm{g\,C\,m^{-2}\,yr^{-1}}$] but within the 95CI of ALT [77.4 – 187.1 $\mathrm{g\,C\,m^{-2}\,yr^{-1}}$]. At SE-Htm (2019 – 2022), mean annual foliage litter production measured at the site was 228.9 $\mathrm{g\,C\,m^{-2}\,yr^{-1}}$, falling within the 95CIs of diagnostic foliage litterfall from both experiments (BAU = [168.9 – 424.5 $\mathrm{g\,C\,m^{-2}\,yr^{-1}}$]; ALT = [163.6 – 299.8 $\mathrm{g\,C\,m^{-2}\,yr^{-1}}$]) but closer to the median ALT estimate (BAU = 297.4 $\mathrm{g\,C\,m^{-2}\,yr^{-1}}$; ALT = 214.1 $\mathrm{g\,C\,m^{-2}\,yr^{-1}}$). No independent litter trap data were available at FI-Var.

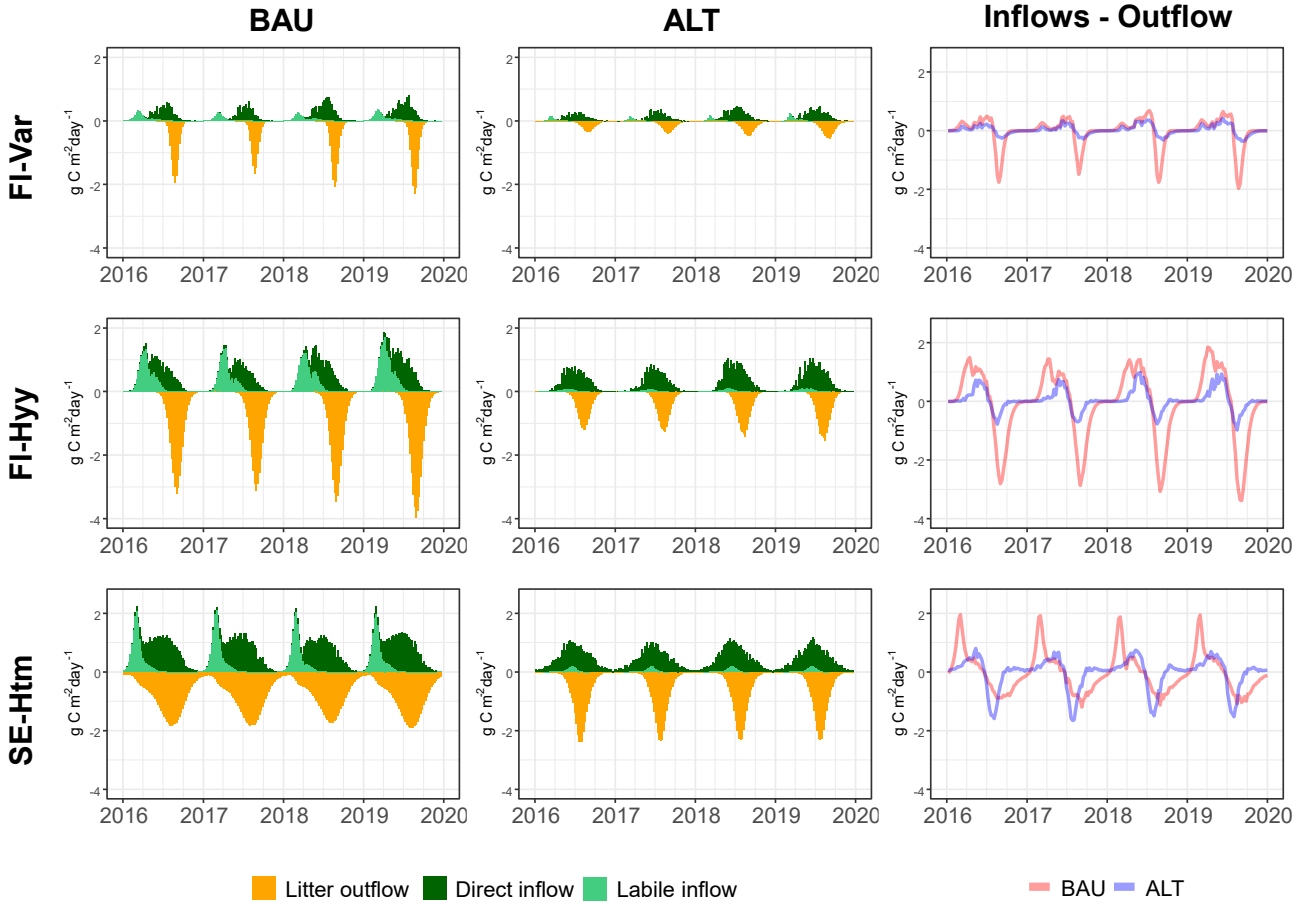

Figure 3. Diagnostic carbon inflows, outflows and net canopy change (inflows – outflow) of the foliage pool stemming from the two assimilation experiments (BAU and ALT) at the three sites in this analysis. Results shown here are based on the median values at each time step.

https://doi.org/10.5194/egusphere-2026-2222
Preprint. Discussion started: 24 April 2026

3.3 Ecosystem functional characteristics

In many cases, functional characteristics retrieved from the two experiments displayed divergent properties (Figure 4). For leaf lifespan, median LL_{BAU} was < 1 year for all three sites (Figure 4a). Median LL_{ALT} mirrored the assimilated leaf lifespan observations, as expected. At all three sites, diagnostic leaf lifespan distributions were statistically dissimilar between the two experiments (Hellinger distance (HD) = 1).

Seasonal biases in assimilated LAI_{EO} observations resulted in higher retrievals of the potential photosynthesis rate (PPR) parameter for the BAU experiments relative to ALT experiments (Figure 4e). Higher PPR_{BAU} allowed low-biased LAI_{BAU} to deliver GPP consistent with assimilated NEE observations during canopy flushing and senescence phases. In contrast, ALT canopies retained leaf area year-round, reducing the need for increased PPR in spring. Median PPR_{BAU} was higher than PPR_{ALT} across all sites; however, distributions of PPR were statistically dissimilar at SE-Htm only (HD = 0.71).

LAI_{EO} biases also impacted diagnostic LMA. LMA_{BAU} was constrained to lower values and median LMA_{ALT} values were higher across all sites. Independent LMA values were closer to LMA_{ALT} at FI-Var and SE-Htm (independent LMA: FI-Var = 97.2 $\mathrm{g\,C\,m^{-2}\,leaf}$; SE-Htm = 117.1 $\mathrm{g\,C\,m^{-2}\,leaf}$). At FI-Hyy, independent LMA (81.8 $\mathrm{g\,C\,m^{-2}\,leaf}$) was more similar to median LMA_{BAU} but fell within 95% CIs for both experiments. LMA distributions were statistically dissimilar between ALT and BAU at all three sites (HD > 0.5).

NPP allocation fractions to the live biomass pools differed between the two experiments, albeit to varying degrees across the sites (Figure 4b,d,f). Across all sites, a larger fraction of NPP_{BAU} were directed to the foliage and labile pools to support the rapid leaf flush signalled from whole-year LAI_{EO}, whereas ALT canopies retained foliage year-round, reducing carbon input requirements. Median fractional NPP_{ALT} allocation to the fine roots was higher than fractional NPP_{BAU} at all sites. Fractional NPP allocation distributions to the canopy and fine roots were not statistically dissimilar at FI-Var, where differences in canopy dynamics were not as pronounced compared to FI-Hyy and SE-Htm (Figure 3). Distributions of diagnostic NPP allocation fraction to wood were dissimilar at SE-Htm only (HD = 0.73).

Carbon use efficiency (CUE = NPP / GPP) was similar between experiments at FI-Var (ALT = 0.38 [0.25 - 0.52]; BAU= 0.42 [0.31 - 0.54]) and FI-Hyy (ALT = 0.57 [0.45 - 0.7]; BAU = 0.54 [0.45 - 0.63]). At SE-Htm, CUE_{ALT} (0.71 [0.58 - 0.79]) was higher than CUE_{BAU} (0.54 [0.46 - 0.64]).

3.4 Biosphere-atmosphere fluxes

BAU and ALT experiments produced similar diagnostics of biosphere-atmosphere carbon fluxes (Figure 5). NEE observations were assimilated in both experiments. GPP and R_{eco} observations were left out for evaluation. RMSE between median diagnostic fluxes and eddy-covariance (EC) values were very similar for both BAU and ALT experiments as both experiments diagnosed nearly indistinguishable component fluxes. Assimilated NEE observations at the southern site, SE-Htm, were much noisier relative to FI-Var and FI-Hyy, and both experiments struggled to fit the fine temporal swings. NEE_{BAU} mean overlap (DOO) with observations was 99% (FI-Var), 93% (FI-Hyy), and 56% (SE-Htm). Similarly, NEE_{ALT} mean overlap was 98% (FI-Var), 95% (FI-Hyy), and 57% (SE-Htm).

https://doi.org/10.5194/egusphere-2026-2222
Preprint. Discussion started: 24 April 2026

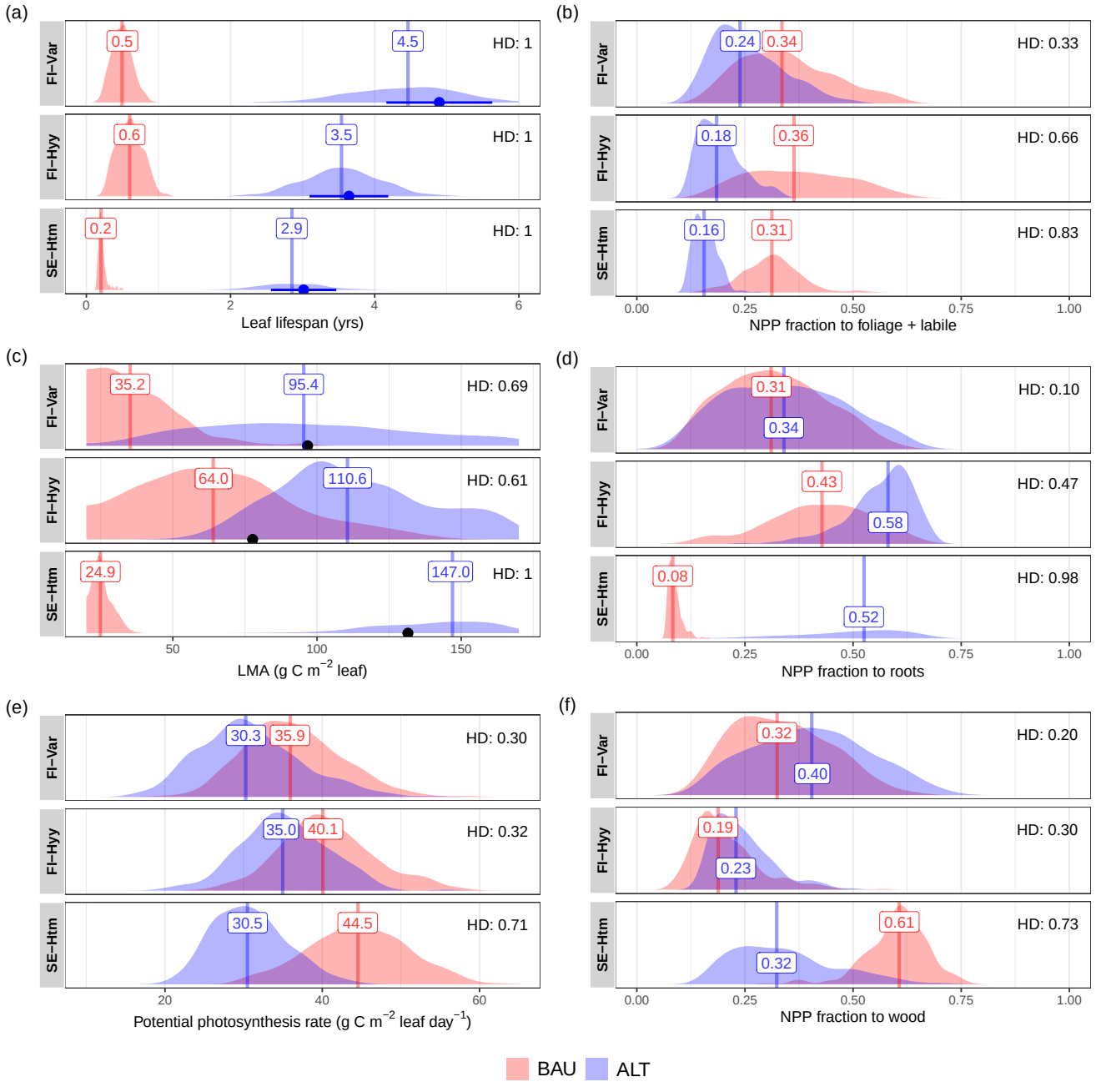

Figure 4. Diagnosed functional characteristics from each assimilation experiment across the three sites. Shown are the posterior distributions from CARDAMOM calibrations of model parameters for leaf lifespan (a), leaf mass per area (c), potential photosynthesis rate (e), and net primary productivity allocation fractions to foliage + labile pools (b), fine roots (d), and wood pools (f). Vertical lines denote median diagnostic values. A Hellinger distance (HD) between the two experiments (BAU, ALT) > 0.5 signifies dissimilar distributions and HD < 0.5 signifies similarity. Blue points in panel (a) show the assimilated leaf lifespan value for ALT experiments. Error bars represent the observational uncertainty. Black points in panel (c) denote independent estimates of effective LMA for evaluation.

https://doi.org/10.5194/egusphere-2026-2222
Preprint. Discussion started: 24 April 2026

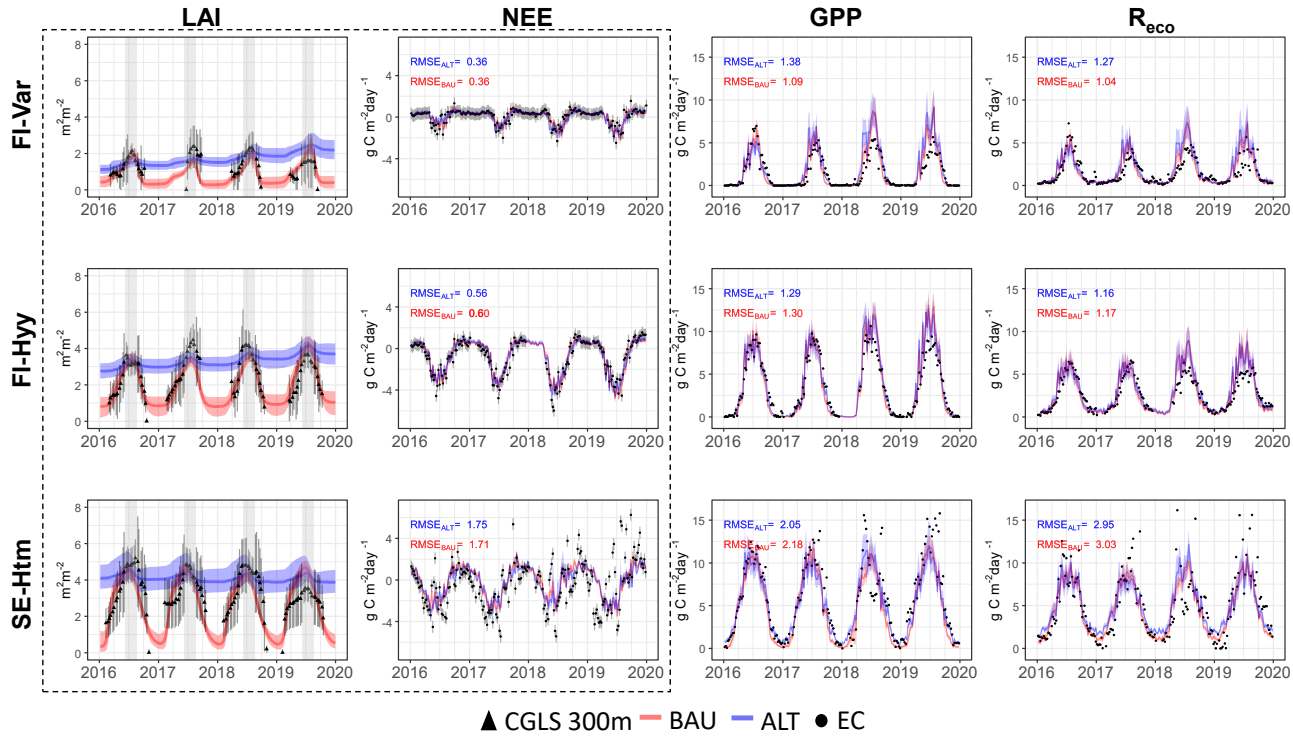

Figure 5. Time series of diagnostic LAI and biosphere-atmosphere carbon fluxes for each experiment (BAU and ALT) across the three sites. Assimilated observations (CGLS 300m LAI and eddy covariance (EC) NEE) are plotted with their uncertainties (error bars, $\pm$ 1 σ), see dashed black box. Grey areas in LAI plots delineate the summer LAI_{EO} assimilation window for the ALT experiment. GPP and R_{eco} were not assimilated in either experiment. Red and blue solid lines represent median diagnostic outputs. Shading represents a 95% confidence interval. RMSE is calculated between median diagnostic fluxes and eddy covariance values (EC).

3.5 Mean annual carbon budgets

Whole-system carbon budgets showed that the number of dissimilar pools and fluxes between the two experiments varied across sites (Figure 6). Dissimilarity is again quantified by the Hellinger distance statistic (HD $>$ 0.5). At FI-Var, carbon cycle differences between BAU and ALT were restricted to three of 22 total components: foliage pool size, foliage litter production ($Mort_{fol}$), and decomposition of litter to SOM (Figure 6a). At FI-Hyy, seven components were statistically dissimilar: NPP allocation to the roots and root litter production ($Mort_{root}$), in addition to canopy related components (Figure 6b). At SE-Htm, 14 components of the carbon cycle were statistically different between BAU and ALT (Figure 6c). Diagnostic pools and fluxes that showed no significant distributional divergence at any of the three sites include: NEE, direct NPP allocation to the foliage pool, size of the wood pool, turnover of the wood pool, size of the SOM pool, and $R_{h\text{-}SOM}$. Of these pools and fluxes, both experiments assimilated NEE, size of the wood pool, and size of the SOM pool. Across all sites, BAU diagnosed higher $Mort_{fol}$:$Mort_{root}$ ratios relative to ALT experiments. At SE-Htm, the ALT experiment resulted in a much higher flow of carbon

https://doi.org/10.5194/egusphere-2026-2222
Preprint. Discussion started: 24 April 2026

from NPP, through the roots and litter pool, to R_h compared to BAU. However, ALT uncertainties were also substantially larger (Figure A1c).

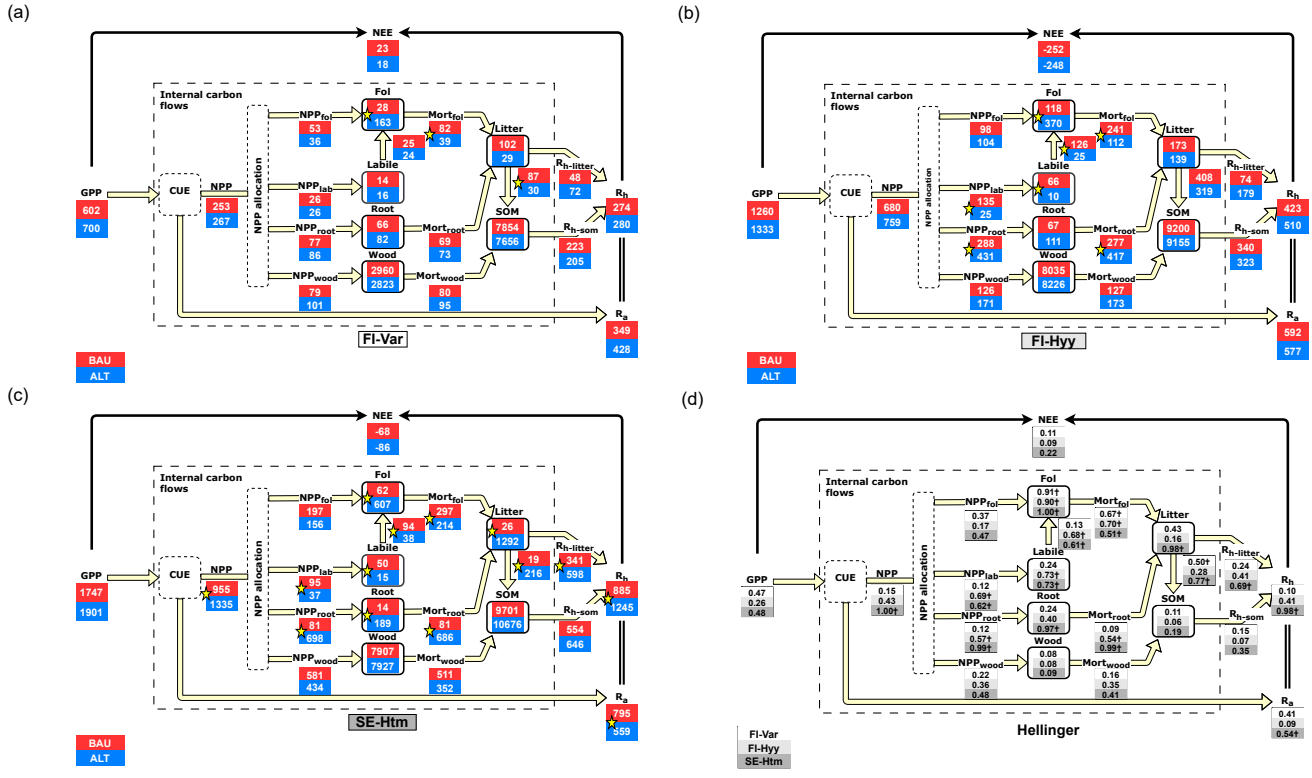

Figure 6. Whole-system carbon cycle schematics for both experiments (BAU and ALT) at each of the three sites. Black boxes indicate mean carbon pools ($g\,C\,m^{-2}$) and arrows represent mean carbon fluxes ($g\,C\,m^{-2}\,yr^{-1}$) across the four-year diagnostic period (2016 – 2019). Values shown are the median ensemble estimates. Stars indicate dissimilarity between distributions of the two experiments (Hellinger distance > 0.5). Panel (d) shows the Hellinger distance values between ALT and BAU experiments at each schematic component, across the three sites († = HD > 0.5).

4 Discussion

Earth observation LAI (LAI_{EO}) show exaggerated seasonal behaviour in evergreen needleleaf forests at northern latitudes compared to in situ data. This seasonal bias was corrected by assimilating information on local leaf lifespan into the CARDAMOM model-data fusion (MDF) framework, alongside observations of LAI limited to the peak growing season (ALT experiment). Experiments showed that seasonal biases in LAI_{EO} impacted diagnosed canopy dynamics with high amounts of carbon transport through the foliage pool each year (BAU experiment). LAI_{EO} biases also affected retrievals of various functional characteristics that erroneously resemble deciduous systems. At southern locations, impacts were not limited to the canopy and biases

https://doi.org/10.5194/egusphere-2026-2222
Preprint. Discussion started: 24 April 2026

propagated throughout the carbon cycle. Despite differences in internal carbon cycling, both ALT and BAU experiments fit observations of biosphere-atmosphere fluxes equally well, highlighting the issue of equifinality. Overall, the inclusion of leaf lifespan as a model calibration constraint led to a more realistic representation of the carbon cycle given the dominance of evergreen needleleaf species at these locations; however, more work is needed to constrain below-ground processes.

4.1 Assimilated leaf lifespan generates realistic LAI seasonality

The ALT assimilation experiment confirmed the hypothesis (H1) that the assimilation of local leaf lifespan information produces more realistic seasonal amplitudes of diagnostic LAI for evergreen needleleaf forests (Figure 2). Assimilated leaf lifespan observations impacted the seasonality of diagnostic LAI by informing canopy turnover rates, and summer-only LAI_{EO} provided constraint on maximum annual leaf area. Rich in situ data sets enabled independent evaluation of leaf lifespan-corrected LAI seasonality generated from a model-data fusion scheme. These field data, and the analysis they enabled here, reinforces the recommendation of Fang et al. (2019) that more LAI_{EO} validation studies are needed with continuous seasonal measurements. Overall, this analysis demonstrates that the assimilation of leaf lifespan and filtering of LAI_{EO} provides a simple correction to LAI_{EO} seasonal biases that enables a more realistic representation of LAI dynamics in evergreen needleleaf forests.

4.2 Earth observation LAI biases propagate into diagnosed functional characteristics and canopy carbon dynamics

The assimilation experiments supported the hypothesis (H2) that naïve assimilation of whole-year LAI_{EO} (BAU experiments) would result in a diagnostic assessment of functional characteristics resembling deciduous systems. This misattribution manifested as short leaf lifespans ($<$ 1 year), low leaf mass per area (LMA) relative to in situ data, and high photosynthetic capacities. In contrast, the assimilation of long leaf lifespans (ALT experiments) induced coordinated shifts in other canopy traits, yielding higher LMA and lower photosynthetic capacity (Figure 4). While both BAU and ALT characteristics represent viable ecological strategies and are consistent with the "fast–slow" axis of the plant economic spectrum, the ALT leaf traits more closely align with evergreen needleleaf expectations (Wright et al., 2004; Reich, 2014; Weng et al., 2017). LAI_{EO} biases also shifted carbon allocation schemes. Fractional NPP_{BAU} allocation to foliage and labile pools was greater than NPP_{ALT} reflecting the need to support annual canopy flushing. Fractional NPP_{BAU} to roots was less than NPP_{ALT} across all sites, aligning with the different root allocation patterns between boreal deciduous and evergreen species reported by Gower et al. (2001).

As expected, seasonal biases in LAI_{EO} also impacted canopy carbon dynamics (Figure 3). BAU canopies were more reliant on labile inputs, which is consistent with the assertion that deciduous species have greater seasonal fluctuations in non-structural carbon (NSC) pools to support canopy flushing relative to conifer species (e.g., Piispanen and Saranpää, 2001; Fischer, 1992; Kramer and Kozlowski, 1979). Independent litter trap data suggest that canopy carbon export in the form of foliage litter production was overestimated in the BAU experiment, driven by the erroneous signal of rapid and substantial autumnal leaf area decline. These results demonstrate that whole-year LAI_{EO} assimilation systematically propagates deciduous-like biases into evergreen systems that distorts both trait retrievals and canopy carbon dynamics.

https://doi.org/10.5194/egusphere-2026-2222
Preprint. Discussion started: 24 April 2026

4.3 Canopy biases from LAI_{EO} propagate to whole-system carbon dynamics

Confirming (H3), the impact of assimilating LAI observations with erroneous seasonality was not limited to the characterisation of canopy dynamics, but further propagated throughout the carbon cycle (Figure 6). Differences between experiments, however, differed across sites/latitude. At the far northern and least productive location (FI-Var), ALT and BAU divergence was less pronounced. FI-Var exhibited the lowest maximum LAI_{EO} across the sites, meaning the maximum potential seasonal biases (in terms of absolute seasonal amplitude, Table 3) were limited relative to the southern sites. Smaller absolute differences in LAI amplitude led to smaller absolute differences in whole-system carbon cycling.

In contrast, at the most southern site (SE-Htm) dissimilarity of mean annual fluxes and pools between experiments was manifold. Strong divergence was driven by two factors: (i) strong biases in canopy carbon dynamics and functional characteristics driven by LAI_{EO} seasonality and (ii) a built-in model constraint on the relationship between foliage and fine root pools. An ecological dynamic constraint (EDC) requires mean annual foliage and fine root pools to be within a factor of five, based on the findings of Mokany et al. (2006). Through the EDC, LAI_{EO} biases propagated into the fine root pool, resulting in an implausibly low and and tightly bound fine root stock BAU estimate (Figures 6 and A1). At a Norway spruce forest in southern Sweden with similar basal area to SE-Htm, Hansson et al. (2013) reported a fine root stock of $351\,\mathrm{g\,C\,m^{-2}}$ (adjusted with a 0.5 biomass to carbon conversion factor). Assuming the reported stock value is representative of SE-Htm, the BAU experiment severely underestimated the fine root pool size [95CI: 63–$116\,\mathrm{g\,C\,m^{-2}}$]. Conversely, the reported stock value fell within the uncertainty range diagnosed by ALT [95CI: 324–$920\,\mathrm{g\,C\,m^{-2}}$]; however, all below-ground ALT uncertainties at SE-Htm were substantial. In some ways though, these high uncertainties signal a more honest representation of below-ground processes in that they are poorly constrained due to a lack of observational data. These uncertainties help identify a key gap in the understanding of ecosystem functioning at this site, whereas the tightly constrained below-ground processes of BAU suggest an over-confident, biased interpretation. The latitudinal gradient of bias propagation across sites suggests that, if assimilated, erroneous LAI_{EO} seasonality may be most impactful for carbon cycle modelling at southern evergreen needleleaf forests with high annual maximum leaf area and carbon stocks.

4.4 Divergent functional characteristics and internal carbon cycling yield indistinguishable biosphere-atmosphere fluxes

Despite significant differences in diagnosed functional characteristics and internal carbon cycling, biosphere-atmosphere fluxes were nearly identical between ALT and BAU experiments across all sites (Figure 5). Similarities in diagnostic NEE are somewhat expected as both experiments assimilated the same observations; however, indistinguishable component fluxes (GPP and R_{eco}) highlight the issue of equifinality. Equifinality arises when very different parameter sets or model structures can lead to the same output (Beven and Freer, 2001). Here, sets of ecologically implausible, deciduous-like characteristics inferred from LAI_{EO} and sets of more realistic evergreen characteristics were shown to be equally capable of generating acceptable agreement with eddy covariance observations. This could suggest validation approaches that rely solely on LAI_{EO} and flux-based observations in northern evergreen needleleaf forests risk drawing flawed ecological interpretations and attributing false con-

https://doi.org/10.5194/egusphere-2026-2222
Preprint. Discussion started: 24 April 2026

fidence in model performance. Moreover, biases in LAI_{EO} can conceal model deficiencies through compensating errors. The incorporation of LAI_{EO} in its current state can lead to correct model outputs for incorrect reasons. Recognising and correcting LAI_{EO} biases is therefore an urgent priority for modelling northern evergreen needleleaf forests.

4.5 Limitations and future directions

This analysis provides new insights into the implications of biased LAI_{EO} for carbon cycle diagnostics. We demonstrate a simple correction method based on leaf lifespan. However, results are subject to a number of limitations that highlight opportunities for future research. Adequately representing below-ground carbon stocks and fluxes continues to be a challenge for the modelling community given the lack of observational constraint (McCormack et al., 2015). Assuming a correct representation of canopy dynamics, indirect constraint on the fine root pool can be achieved by providing information on foliage-to-fine root ratios. The default EDC on foliage-to-fine root ratio used here was designed for global applications and proved overly broad in this context. Moving forward, CARDAMOM could incorporate region-specific data on foliage-to-fine root ratios to better constrain below-ground dynamics (e.g., Helmisaari et al., 2007; Vanninen and Mäkelä, 1999). Additionally, this study was restricted to only three sites, limiting the ability to assess LAI_{EO} impacts across broader climatic and ecological gradients. Future work could expand the spatial scope to investigate bias propagation across a range of forest structures and species mixtures. Additionally, it remains to be seen whether the assimilation of leaf lifespan can consistently enhance model realism across large spatial scales.

5 Conclusions

LAI observations from Earth observation exhibit erroneous, strong seasonal amplitudes over northern evergreen needleleaf forests that are functionally inconsistent with the ecological traits and carbon dynamics of these ecosystems. This analysis shows that incorporating leaf lifespan information within a data assimilation scheme provides a simple, yet effective method to correct these biases. When left uncorrected, biased LAI_{EO} observations have significant impacts on diagnoses of carbon cycle dynamics. Despite divergences in diagnostic functional characteristics and internal carbon cycling, corrected and uncorrected LAI experiments generated very similar outputs of biosphere-atmosphere fluxes. Studies that incorporate uncorrected LAI_{EO} in analyses of these forests may therefore be unknowingly inheriting biases into their results that may not be apparent if validating against a limited number of commonly used data streams. By obscuring ecological realism while preserving flux agreement, assimilation of LAI_{EO} may compromise the ability to accurately represent and understand carbon cycling in this important region of high carbon storage and rapid climate change.

Code and data availability. The driving data and selected carbon cycle outputs have been archived (Green et al., 2026) at Edinburgh DataShare: https://doi.org/10.7488/ds/8116. Model and analysis code will be made available pending manuscript acceptance.

https://doi.org/10.5194/egusphere-2026-2222
Preprint. Discussion started: 24 April 2026

Author contributions. TJG and MW formulated the experimental design. TJG ran the CARDAMOM experiments and analysed the outputs. TJG wrote the original draft. DTM, TLS, AM, and MW reviewed and editied the manuscript.

Competing interests. The authors declare no competing interests.

Acknowledgements. The authors would like to extend a special thank you to the ICOS personnel Tobias Biermann (site manager, SE-Htm) and Pasi Kolari (site PI, FI-Var and data manager, FI-Hyy) for providing the field data and input on the manuscript. T. J. Green was funded by the University of Edinburgh and University of Helsinki Partnership Programme on Forests. D. T. Milodowski was funded by the UKRI as part of the SECO project (NE/T01279X/1). T. L. Smallman and M. Williams were funded by the NERC's National Centre for Earth Observation (NE/R016518/1). T. L. Smallman was additionally funded by the UK's Earth Observation Climate Information Service (NE/X019071/1).

https://doi.org/10.5194/egusphere-2026-2222
Preprint. Discussion started: 24 April 2026

Appendix A

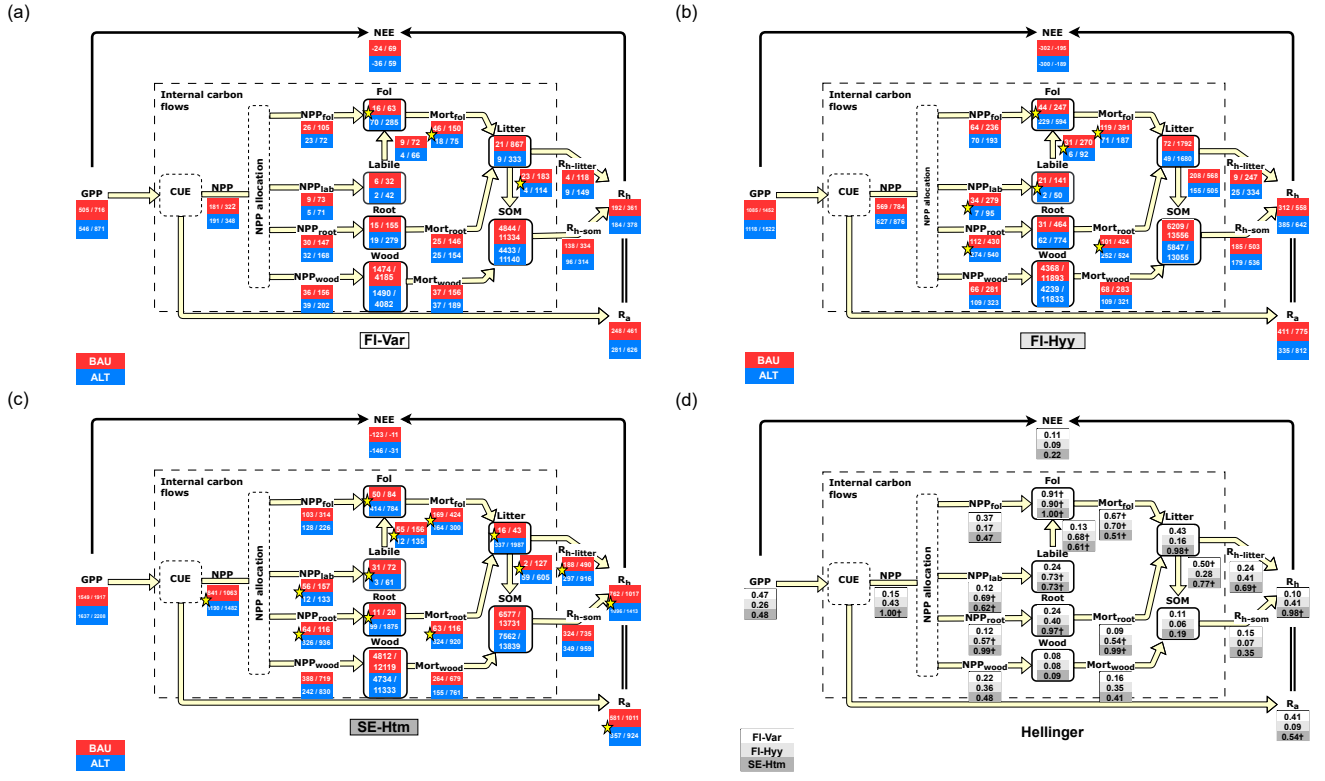

Figure A1. Uncertainty of whole-system carbon cycle schematics for both experiments (BAU and ALT) at each of the three sites. Black boxes indicate mean carbon pools ($g\,C\,m^{-2}$) and arrows represent mean carbon fluxes ($g\,C\,m^{-2}\,yr^{-1}$) across the four-year diagnostic period (2016 – 2019). Values shown are the lower and upper bounds of a 95% confidence interval based on 300-member ensembles. Stars indicate dissimilarity between distributions of the two experiments (Hellinger distance > 0.5). Panel (d) shows the Hellinger distance values between ALT and BAU experiments at each schematic component across the three sites († = HD > 0.5).

https://doi.org/10.5194/egusphere-2026-2222
Preprint. Discussion started: 24 April 2026

Description	Units	Minimum value	Maximum value
Decomposition of litter to SOM	$g\,C\,m^{-2}\,day^{-1}$	1e-5	0.01
*Fraction of GPP respired as R_a (R_a:GPP)	fraction	0.2	0.8
Fraction of GPP to labile pool ($Frac_{lab}$)	fraction	0.01	0.5
Fraction of GPP to fine roots ($Frac_{root}$)	fraction	0.1	0.8
Fraction of GPP to foliage ($Frac_{fol}$)	fraction	0.1	0.5
Turnover of wood	fraction day^{-1}	9e–6 (304.2 yrs)	0.001 (2.7 yrs)
Turnover of fine roots	fraction day^{-1}	8.91e–4 (3.1[a] yrs)	0.02 (0.1 yrs)
Turnover of foliage	fraction $year^{-1}$	7.69e–2 (13[b] yrs)	1 (1 year)
Mineralisation of litter	fraction day^{-1}	1.11e–4 (24 yrs at 0° C)	0.02 (0.1 yrs at 0° C)
Mineralisation of SOM	fraction day^{-1}	1.37e–6 (2000 yrs at 0° C)	9.13e–5 (30 yrs at 0° C)
R_h exponential temperature response	–	0.019	0.08
*Potential photosynthesis rate (PPR)	$g\,C\,m^{-2}\,leaf\,day^{-1}$	1.64	100
Maximum bud burst timing	day of year	60	183
Labile release period	days	10	100
Maximum leaf fall timing	day of year	183	365
Leaf fall duration	days	20	150
Leaf mass per area	$g\,C\,m^{-2}\,leaf$	20	180
Coarse root fraction of wood pool	fraction	0.15	0.5
Coarse root biomass to reach 50% max rooting depth	g dry matter m^{-2}	100	2500
Maximum (coarse) rooting depth	meters	0.35	4
Initial labile pool size	$g\,C\,m^{-2}$	1	2000
Initial foliage pool size	$g\,C\,m^{-2}$	1	2000
Initial fine root pool size	$g\,C\,m^{-2}$	1	2000
Initial wood pool size	$g\,C\,m^{-2}$	1	30000
Initial litter pool size	$g\,C\,m^{-2}$	1	2000
Initial SOM pool size	$g\,C\,m^{-2}$	200	250000
Initial soil water	fraction of field capacity	0.5	1

Table A1. DALEC parameter descriptions, units and prior ranges. [a] value based on Hansson et al. (2013). [b] value based on Tupek et al. (2015). Values in ( ) show the equivalent residence times of the turnover rates. * denotes parameters with additional constraint (see Section 2.1.2). GPP = gross primary productivity; R_a = autotrophic respiration; R_h = heterotrophic respiration; SOM = soil organic matter. Fractional allocation of GPP is applied sequentially. Absolute GPP allocation to wood = GPP - (GPP·R_a:GPP) - (GPP·$Frac_{lab}$) - (GPP·$Frac_{root}$) - (GPP·$Frac_{fol}$).

https://doi.org/10.5194/egusphere-2026-2222
Preprint. Discussion started: 24 April 2026

References

Aslan, T., Launiainen, S., Kolari, P., Peltola, O., Aalto, J., Bäck, J., Vesala, T., and Mammarella, I.: Thinning turned boreal forest to a carbon source - short term effects of partial harvest on carbon dioxide and water vapor fluxes, Agricultural and Forest Meteorology, 353, https://doi.org/10.1016/j.agrformet.2024.110061, 2024.

Baldocchi, D.: Assessing the eddy covariance technique for evaluating carbon dioxide exchange rates of ecosystems: past, present and future, Global Change Biology, 9, 479–492, https://doi.org/10.1046/j.1365-2486.2003.00629.x, 2003.

Baret, F., Hagolle, O., Geiger, B., Bicheron, P., Miras, B., Huc, M., Berthelot, B., Niño, F., Weiss, M., and Samain, O.: LAI, fAPAR and fCover CYCLOPES global products derived from VEGETATION: Part 1: Principles of the algorithm, Remote Sensing of Environment, 110, 275–286, https://doi.org/10.1016/j.rse.2007.02.018, 2007.

Baret, F., Weiss, M., Verger, A., and Smets, B.: ATBD for LAI, FAPAR and FCOVER from PROBA-V products at 300 m resolution (Geov3), Tech. rep., Institut National de la Recherche Agronomique, https://www.fp7-imagines.eu/media/Documents/ImagineS_RP2.1_ATBD-LAI300m_I1.73.pdf, 2016.

Beven, K. and Freer, J.: Equifinality, data assimilation, and uncertainty estimation in mechanistic modelling of complex environmental systems using the GLUE methodology, Journal of Hydrology, 249, 11–29, https://doi.org/10.1016/S0022-1694(01)00421-8, 2001.

Bloom, A. and Williams, M.: Constraining ecosystem carbon dynamics in a data-limited world: integrating ecological "common sense" in a model–data fusion framework, Biogeosciences, 12, 1299–1315, https://doi.org/10.5194/bg-12-1299-2015, 2015.

Bloom, A., Exbrayat, J., Van Der Velde, I., Feng, L., and Williams, M.: The decadal state of the terrestrial carbon cycle: Global retrievals of terrestrial carbon allocation, pools, and residence times, Proceedings of the National Academy of Sciences, 113, 1285–1290, https://doi.org/10.1073/pnas.1515160113, 2016.

Boone, E., Merrick, J., and Krachey, M.: A Hellinger distance approach to MCMC diagnostics, Journal of Statistical Computation and Simulation, 84, 833–849, https://doi.org/10.1080/00949655.2012.729588, 2014.

Bradshaw, C. and Warkentin, I.: Global estimates of boreal forest carbon stocks and flux, Global and Planetary Change, 128, 24–30, https://doi.org/10.1016/j.gloplacha.2015.02.004, 2015.

Brown, L., Meier, C., Morris, H., Pastor-Guzman, J., Bai, G., Lerebourg, C., Gobron, N., Lanconelli, C., Clerici, M., and Dash, J.: Evaluation of global leaf area index and fraction of absorbed photosynthetically active radiation products over North America using Copernicus Ground Based Observations for Validation data, Remote Sensing of Environment, 247, https://doi.org/10.1016/j.rse.2020.111935, 2020.

Chen, J.: Optically-based methods for measuring seasonal variation of leaf area index in boreal conifer stands, Agricultural and Forest Meteorology, 80, 135–163, https://doi.org/10.1016/0168-1923(95)02291-0, 1996.

Chen, J. and Black, T.: Defining leaf area index for non-flat leaves, Plant, Cell and Environment, 15, 421–429, https://doi.org/10.1111/j.1365-3040.1992.tb00992.x, 1992.

Chianucci, F.: An overview of in situ digital canopy photography in forestry, Canadian Journal of Forest Research, 50, 227–242, https://doi.org/10.1139/cjfr-2019-0055, 2020.

Cohen, W., Maiersperger, T., Turner, D., Ritts, W., Pflugmacher, D., Kennedy, R., Kirschbaum, A., Running, S., Costa, M., and Gower, S.: MODIS land cover and LAI collection 4 product quality across nine sites in the western hemisphere, IEEE Transactions on Geoscience and Remote Sensing, 44, 1843–1857, https://doi.org/10.1109/tgrs.2006.876026, 2006.

Collalti, A. and Prentice, I.: Is NPP proportional to GPP? Waring's hypothesis 20 years on, Tree physiology, 39, 1473–1483, https://doi.org/10.1093/treephys/tpz034, 2019.

https://doi.org/10.5194/egusphere-2026-2222
Preprint. Discussion started: 24 April 2026

Famiglietti, C., Smallman, T., Levine, P., Flack-Prain, S., Quetin, G., Meyer, V., Parazoo, N., Stettz, S., Yang, Y., and Bonal, D.: Optimal model complexity for terrestrial carbon cycle prediction, Biogeosciences, 18, 2727–2754, https://doi.org/10.5194/bg-18-2727-2021, 2021.

Fang, H., Baret, F., Plummer, S., and Schaepman-Strub, G.: An Overview of Global Leaf Area Index (LAI): Methods, Products, Validation, and Applications, Reviews of Geophysics, 57, 739–799, https://doi.org/10.1029/2018rg000608, 2019.

Fang, H., Li, S.and Zhang, Y., Wei, S., and Wang, Y.: New insights of global vegetation structural properties through an analysis of canopy clumping index, fractional vegetation cover, and leaf area index, Science of Remote Sensing, 4, https://doi.org/10.1016/j.srs.2021.100027, 2021.

Fischer, C.and Höll, W.: Food reserves of scots pine (*Pinus sylvestris* L.) II. Seasonal changes and radial distribution of carbohydrate and fat reserves in pine wood, Trees, 6, 147–155, https://doi.org/10.1007/BF00202430, 1992.

Fisher, J., Huntzinger, D., Schwalm, C., and Sitch, S.: Modeling the Terrestrial Biosphere, Annual Review of Environment and Resources, 39, 91–123, https://doi.org/10.1146/annurev-environ-012913-093456, 2014.

Friedlingstein, P., Meinshausen, M., Arora, V., Jones, C., Anav, A., Liddicoat, S., and Knutti, R.: Uncertainties in CMIP5 Climate Projections due to Carbon Cycle Feedbacks, Journal of Climate, 27, 511–526, https://doi.org/10.1175/jcli-d-12-00579.1, 2014.

Fuster, B., Sánchez-Zapero, J., Camacho, F., García-Santos, V., Verger, A., Lacaze, R., Weiss, M., Baret, F., and Smets, B.: Quality assessment of PROBA-V LAI, fAPAR and fCOVER collection 300 m products of copernicus global land service, Remote Sensing, 12, 1017, https://doi.org/10.3390/rs12061017, 2020.

Garrigues, S., Lacaze, R., Baret, F., Morisette, J., Weiss, M., Nickeson, J., Fernandes, R., Plummer, S., Shabanov, N., Myneni, R., et al.: Validation and intercomparison of global Leaf Area Index products derived from remote sensing data, Journal of Geophysical Research: Biogeosciences, 113, https://doi.org/10.1029/2007JG000635, 2008.

Gielen, B., Op de Beeck, M., Michilsens, F., and Papale, D.: ICOS Ecosystem Instructions for Ancillary Vegetation Measurements in Forest (Version 20200330), ICOS Ecosystem Thematic Centre, https://doi.org/10.18160/4ajs-z4r9, 2017.

Gower, S., Krankina, O., Olson, R., Apps, M., Linder, S., and Wang, C.: Net primary production and carbon allocation patterns of boreal forest ecosystems, Ecological Applications, 11, 1395–1411, https://doi.org/10.1890/1051-0761(2001)011[1395:NPPACA]2.0.CO;2, 2001.

Green, T., Milodowski, D., Smallman, T., Mäkelä, A., and Williams, M.: CARDAMOM driving data and model outputs to accompany "Spurious seasonality of Earth observation LAI across three northern evergreen needleleaf forests: Implications for analyses of the carbon cycle", https://doi.org/10.7488/ds/8116, 2026.

Haario, H., Saksman, E., and Tamminen, J.: An adaptive Metropolis algorithm, Bernoulli, 7, 223–242, 2001.

Hansson, K., Helmisaari, H., Sah, S., and Lange, H.: Fine root production and turnover of tree and understorey vegetation in Scots pine, silver birch and Norway spruce stands in SW Sweden, Forest Ecology and Management, 309, 58–65, https://doi.org/10.1016/j.foreco.2013.01.022, 2013.

Heiskanen, J., Rautiainen, M., Stenberg, P., Mõttus, M., Vesanto, V., Korhonen, L., and Majasalmi, T.: Seasonal variation in MODIS LAI for a boreal forest area in Finland, Remote Sensing of Environment, 126, 104–115, https://doi.org/10.1016/j.rse.2012.08.001, 2012.

Heliasz, M., Kljun, N., Biermann, T., Holst, J., Holst, T., Kornacher, P., Linderson, M., Mölder, M., and Rinne, J.: ETC L2 ARCHIVE from Hyltemossa, 2018–2025, https://hdl.handle.net/11676/RqQ6UrHcHscdwQ4lfU39bd-6, 2026.

Hellinger, E.: Neue begründung der theorie quadratischer formen von unendlichvielen veränderlichen, Journal für die reine und angewandte Mathematik, 1909, 210–271, http://eudml.org/doc/149313, 1909.

Helmisaari, H., Derome, J., Nojd, P., and Kukkola, M.: Fine root biomass in relation to site and stand characteristics in Norway spruce and Scots pine stands, Tree Physiology, 27, 1493–1504, https://doi.org/10.1093/treephys/27.10.1493, 2007.

https://doi.org/10.5194/egusphere-2026-2222
Preprint. Discussion started: 24 April 2026

Hill, T., Ryan, E., and Williams, M.: The use of CO2 flux time series for parameter and carbon stock estimation in carbon cycle research, Global Change Biology, 18, 179–193, https://doi.org/10.1111/j.1365-2486.2011.02511.x, 2012.

Jankowski, A., Wyka, T., Żytkowiak, R., Nihlgård, B., Reich, P., and Oleksyn, J.: Cold adaptation drives variability in needle structure and anatomy in *Pinus sylvestris* L. along a 1,900 km temperate–boreal transect, Functional Ecology, 31, 2212–2223, https://doi.org/10.1111/1365-2435.12946, 2017.

Jarlan, L., Balsamo, G., Lafont, S., Beljaars, A., Calvet, J., and Mougin, E.: Analysis of leaf area index in the ECMWF land surface model and impact on latent heat and carbon fluxes: Application to West Africa, Journal of Geophysical Research: Atmospheres, 113, https://doi.org/10.1029/2007JD009370, 2008.

Jones, M.: Simple boundary correction for kernel density estimation, Statistics and Computing, 3, 135–146, https://doi.org/10.1007/BF00147776, 1993.

Kattge, J., Bönisch, G., Díaz, S., Lavorel, S., Prentice, I., Leadley, P., Tautenhahn, S., Werner, G., Aakala, T., Abedi, M., et al.: TRY plant trait database–enhanced coverage and open access, Global change biology, 26, 119–188, https://doi.org/10.1111/gcb.14904, 2020.

Keenan, T., Davidson, E., Moffat, A., Munger, W., and Richardson, A.: Using model-data fusion to interpret past trends, and quantify uncertainties in future projections, of terrestrial ecosystem carbon cycling, Global Change Biology, 18, 2555–2569, https://doi.org/10.1111/j.1365-2486.2012.02684.x, 2012.

Kramer, P. and Kozlowski, T.: Physiology of woody plants, Academic Press, Orlando, Florida, USA, 1979.

Lasslop, G., Reichstein, M., Papale, D., Richardson, A., Arneth, A., Barr, A., Stoy, P., and Wohlfahrt, G.: Separation of net ecosystem exchange into assimilation and respiration using a light response curve approach: critical issues and global evaluation, Global Change Biology, 16, 187–208, https://doi.org/10.1111/j.1365-2486.2009.02041.x, 2010.

Li, X., Du, H., Mao, F., Zhou, G., Han, N., Xu, X., Liu, Y., Zhu, D., Zheng, J., and Dong, L.: Assimilating spatiotemporal MODIS LAI data with a particle filter algorithm for improving carbon cycle simulations for bamboo forest ecosystems, Science of the Total Environment, 694, 133 803, https://doi.org/10.1016/j.scitotenv.2019.133803, 2019.

MacBean, N., Peylin, P., Chevallier, F., Scholze, M., and Schürmann, G.: Consistent assimilation of multiple data streams in a carbon cycle data assimilation system, Geoscientific Model Development, 9, 3569–3588, https://doi.org/10.5194/gmd-9-3569-2016, 2016.

Mäkelä, A., Kolari, P., Karimäki, J., Nikinmaa, E., Perämäki, M., and Hari, P.: Modelling five years of weather-driven variation of GPP in a boreal forest, Agricultural and Forest Meteorology, 139, 382–398, https://doi.org/10.1016/j.agrformet.2006.08.017, 2006.

Marklund, L.: Biomass functions for pine, spruce and birch in Sweden, Rapport-Sveriges Lantbruksuniversitet, Institutionen foer Skogstaxering (Sweden), 1988.

McCormack, M., Crisfield, E., Raczka, B., Schnekenburger, F., Eissenstat, D., and Smithwick, E.: Sensitivity of four ecological models to adjustments in fine root turnover rate, Ecological Modelling, 297, 107–117, https://doi.org/10.1016/j.ecolmodel.2014.11.013, 2015.

Mokany, K., Raison, R., and Prokushkin, A.: Critical analysis of root: shoot ratios in terrestrial biomes, Global Change Biology, 12, 84–96, https://doi.org/10.1111/j.1365-2486.2005.001043.x, 2006.

Muukkonen, P.: Needle biomass turnover rates of Scots pine (*Pinus sylvestris* L.) derived from the needle-shed dynamics, Trees, 19, 273–279, https://doi.org/10.1007/s00468-004-0381-4, 2005.

Myneni, R., Knyazikhin, Y., and Park, T.: MODIS/Terra Leaf Area Index/FPAR 8-Day L4 Global 500m SIN Grid V061, NASA EOSDIS Land Processes Distributed Active Archive Center (DAAC) data set, p. MCD15A2H. 061, 2021.

Oleksyn, J., Wyka, T., Zytkowiak, R., Zadworny, M., Mucha, J., Dering, M., Ufnalski, K., Nihlgård, B., and Reich, P.: A fingerprint of climate change across pine forests of Sweden, Ecology Letters, 23, 1739–1746, https://doi.org/10.1111/ele.13587, 2020.

https://doi.org/10.5194/egusphere-2026-2222
Preprint. Discussion started: 24 April 2026

Pan, Y., Birdsey, R., Phillips, O., Houghton, R., Fang, J., Kauppi, P., Keith, H., Kurz, W., Ito, A., Lewis, S., Nabuurs, G., Shvidenko, A., Hashimoto, S., Lerink, B., Schepaschenko, D., Castanho, A., and Murdiyarso, D.: The enduring world forest carbon sink, Nature, 631, 563–569, https://doi.org/10.1038/s41586-024-07602-x, 2024.

Petersson, H. and Ståhl, G.: Functions for below-ground biomass of *Pinus sylvestris*, *Picea abies*, *Betula pendula* and *Betula pubescens* in Sweden, Scandinavian Journal of Forest Research, 21, 84–93, https://doi.org/10.1080/14004080500486864, 2006.

Piao, S., Wang, X., Wang, K., Li, X., Bastos, A.and Canadell, J., Ciais, P., Friedlingstein, P., and Sitch, S.: Interannual variation of terrestrial carbon cycle: Issues and perspectives, Global Change Biology, 26, 300–318, https://doi.org/10.1111/gcb.14884, 2020.

Piispanen, R. and Saranpää, P.: Variation of non-structural carbohydrates in silver birch (*Betula pendula* Roth) wood, Trees, 15, 444–451, https://doi.org/10.1007/s004680100125, 2001.

Poggio, L., De Sousa, L., Batjes, N., Heuvelink, G., Kempen, B., Ribeiro, E., and Rossiter, D.: SoilGrids 2.0: producing soil information for the globe with quantified spatial uncertainty, SOIL, 7, 217–240, https://doi.org/10.5194/soil-7-217-2021, 2021.

Post, E., Alley, R., Christensen, T., Macias-Fauria, M., Forbes, B., Gooseff, M., Iler, A., Kerby, J., Laidre, K., and Mann, M.: The polar regions in a 2° C warmer world, Science Advances, 5, eaaw9883, https://doi.org/10.1126/sciadv.aaw9883, 2019.

Reich, P.: The world-wide 'fast–slow' plant economics spectrum: a traits manifesto, Journal of Ecology, 102, 275–301, https://doi.org/10.1111/1365-2745.12211, 2014.

Reich, P., Walters, M., and Ellsworth, D.: Leaf life-span in relation to leaf, plant, and stand characteristics among diverse ecosystems, Ecological Monographs, 62, 365–392, https://doi.org/10.2307/2937116, 1992.

Reich, P., Rich, R., Lu, X., Wang, Y., and Oleksyn, J.: Biogeographic variation in evergreen conifer needle longevity and impacts on boreal forest carbon cycle projections, Proceedings of the National Academy of Sciences, 111, 13 703–13 708, https://doi.org/10.1073/pnas.1216054110, 2014.

Reichstein, M., Falge, E., Baldocchi, D., Papale, D., Aubinet, M., Berbigier, P., Bernhofer, C., Buchmann, N., Gilmanov, T., and Granier, A.: On the separation of net ecosystem exchange into assimilation and ecosystem respiration: review and improved algorithm, Global Change Biology, 11, 1424–1439, https://doi.org/10.1111/j.1365-2486.2005.001002.x, 2005.

Scholze, M., Buchwitz, M., Dorigo, W., Guanter, L., and Quegan, S.: Reviews and syntheses: Systematic Earth observations for use in terrestrial carbon cycle data assimilation systems, Biogeosciences, 14, 3401–3429, https://doi.org/10.5194/bg-14-3401-2017, 2017.

Sheather, S. and Jones, M.: A reliable data-based bandwidth selection method for kernel density estimation, Journal of the Royal Statistical Society, 53, 683–690, https://doi.org/10.1111/j.2517-6161.1991.tb01857.x, 1991.

Smallman, T. and Williams, M.: Description and validation of an intermediate complexity model for ecosystem photosynthesis and evapotranspiration: ACM-GPP-ETv1, Geoscientific Model Development, 12, 2227–2253, https://doi.org/10.5194/gmd-12-2227-2019, 2019.

Smallman, T., Milodowski, D., Neto, E., Koren, G., Ometto, J., and Williams, M.: Parameter uncertainty dominates C cycle forecast errors over most of Brazil for the 21st Century, Earth System Dynamics Discussions, 2021, 1–52, https://doi.org/10.5194/esd-12-1191-2021, 2021.

Smith, N.: Estimating leaf area index and light extinction coefficients in stands of Douglas-fir (*Pseudotsuga menziesii*), Canadian Journal of Forest Research, 23, 317–321, https://doi.org/10.1139/x93-043, 1993.

Tian, Y., Dickinson, R., Zhou, L., Zeng, X., Dai, Y., Myneni, R., Knyazikhin, Y., Zhang, X., Friedl, M., Yu, H., et al.: Comparison of seasonal and spatial variations of leaf area index and fraction of absorbed photosynthetically active radiation from Moderate Resolution Imaging Spectroradiometer (MODIS) and Common Land Model, Journal of Geophysical Research, 109, https://doi.org/10.1029/2003jd003777, 2004.

https://doi.org/10.5194/egusphere-2026-2222
Preprint. Discussion started: 24 April 2026

Tupek, B., Mäkipää, R., Heikkinen, J., Peltoniemi, M., Ukonmaanaho, L., Hokkanen, T., Nöjd, P., Nevalainen, S., Lindgren, M., and Lehtonen, A.: Foliar turnover rates in Finland-comparing estimates from needle-cohort and litterfall-biomass methods, Boreal Environment Research, 20, 283–304, http://hdl.handle.net/10138/165220, 2015.

Vanninen, P. and Mäkelä, A.: Fine root biomass of Scots pine stands differing in age and soil fertility in southern Finland, Tree Physiology, 19, 823–830, https://doi.org/10.1093/treephys/19.12.823, 1999.

Venäläinen, A. and Nordlund, A.: Kasvukauden ilmastotiedotteen sisältö ja käyttö (Contents and use of the climatological report of a growing season, in Finnish), Finnish Meteorological Institute Reports, 6, 1988.

Verger, A., Filella, I., and Baret, F.and Peñuelas, J.: Vegetation baseline phenology from kilometric global LAI satellite products, Remote Sensing of Environment, 178, 1–14, https://doi.org/10.1016/j.rse.2016.02.057, 2016.

Wang, R., Chen, J., Liu, Z., and Arain, A.: Evaluation of seasonal variations of remotely sensed leaf area index over five evergreen coniferous forests, ISPRS Journal of Photogrammetry and Remote Sensing, 130, 187–201, https://doi.org/10.1016/j.isprsjprs.2017.05.017, 2017.

Wang, Y., Trudinger, C., and Enting, I.: A review of applications of model–data fusion to studies of terrestrial carbon fluxes at different scales, Agricultural and Forest Meteorology, 149, 1829–1842, https://doi.org/10.1016/j.agrformet.2009.07.009, 2009.

Warm Winter Team and ICOS Ecosystem Thematic Center: Warm Winter 2020 ecosystem eddy covariance flux product for 73 stations in FLUXNET-Archive format—release 2022-1, https://doi.org/10.18160/2G60-ZHAK, 2020.

Weiss, M., Baret, F., Garrigues, S., and Lacaze, R.: LAI and fAPAR CYCLOPES global products derived from VEGETATION. Part 2: Validation and comparison with MODIS collection 4 products, Remote Sensing of Environment, 110, 317–331, https://doi.org/10.1016/j.rse.2007.03.001, 2007.

Weng, E., Farrior, C., Dybzinski, R., and Pacala, S.: Predicting vegetation type through physiological and environmental interactions with leaf traits: evergreen and deciduous forests in an earth system modeling framework, Global change biology, 23, 2482–2498, https://doi.org/10.1111/gcb.13542, 2017.

Williams, M., Schwarz, P., Law, B., Irvine, J., and Kurpius, M.: An improved analysis of forest carbon dynamics using data assimilation, Global Change Biology, 11, 89—-105, https://doi.org/10.1111/j.1365-2486.2004.00891.x, 2005.

WMO, UNESCO, IOC, UNEP, and ISC: The 2022 GCOS ECVs Requirements, Tech. rep., World Meteorological Organization, Geneva, https://library.wmo.int/idurl/4/58111, 2022.

Worden, M., Bilir, T., Bloom, A., Fang, J., Klinek, L., Konings, A., Levine, P., Milodowski, D., Quetin, G., Smallman, T., Bar-On, Y., Braghiere, R., David, C., Fischer, N., Gentine, P., Green, T., Jones, A., Liu, J., Longo, M., Ma, S., Magney, T., Massoud, E., Myrgiotis, V., Norton, A., Parazoo, N., Tajfar, E., Trugman, A., Williams, M., Worden, S., Zhao, W., and Zhu, S.: Combining Observations and Models: A Review of the CARDAMOM Framework for Data-Constrained Terrestrial Ecosystem Modeling, Global Change Biology, 31, e70 462, https://doi.org/10.1111/gcb.70462, 2025.

Wright, I., Reich, P., Westoby, M., Ackerly, D., Baruch, Z., Bongers, F., Cavender-Bares, J., Chapin, T., Cornelissen, J., Diemer, M., Flexas, J.and Garnier, E., Groom, P., Gulias, J., Hikosaka, K., Lamont, B., Lee, T., Lee, W., Lusk, C., Midgley, J., Navas, M., Niinemets, U., Oleksyn, J., Osada, N., Poorter, H., Poot, P., Prior, L., Pyankov, V., Roumet, C., Thomas, S., Tjoelker, M., Veneklaas, E., and Villar, R.: The worldwide leaf economics spectrum, Nature, 428, 821–827, https://doi.org/10.1038/nature02403, 2004.

Xiao, J., Davis, K., Urban, N., and Keller, K.: Uncertainty in model parameters and regional carbon fluxes: A model-data fusion approach, Agricultural and Forest Meteorology, 189, 175–186, https://doi.org/10.1016/j.agrformet.2014.01.022, 2014.

Yan, K., Park, T., Yan, G., Chen, C., Yang, B., Liu, Z., Nemani, R., Knyazikhin, Y., and Myneni, R.: Evaluation of MODIS LAI/FPAR product collection 6. Part 1: Consistency and improvements, Remote Sensing, 8, 359, https://doi.org/10.3390/rs8050359, 2016.

https://doi.org/10.5194/egusphere-2026-2222
Preprint. Discussion started: 24 April 2026

Yang, W., Shabanov, N., Huang, D., Wang, W., Dickinson, R., Nemani, R., Knyazikhin, Y., and Myneni, R.: Analysis of leaf area index products from combination of MODIS Terra and Aqua data, Remote Sensing of Environment, 104, 297–312, https://doi.org/10.1016/j.rse.2006.04.016, 2006.